

1  
2  
3 **The Myc-Like Mlx Network Impacts Aging and Metabolism**  
4  
5  
6  
7

8 **Short title: The Mlx Network Impacts Aging and Metabolism**  
9

10  
11  
12 Key words: Cancer metabolism, DNA damage, mitochondria, Myc, reactive oxygen species, telomeres,  
13 Warburg effect, TCA cycle  
14

15  
16  
17 Huabo Wang<sup>1</sup>, Taylor Stevens<sup>1</sup>, Jie Lu<sup>1</sup>, Alexander Roberts<sup>1</sup>, Clinton Van't Land<sup>2</sup>, Radhika Muzumdar<sup>3</sup>,  
18 Zhenwei Gong<sup>3</sup>, Jerry Vockley<sup>2</sup>, Edward V. Prochownik<sup>1,4,5,6,7</sup>  
19

20  
21  
22  
23  
24 <sup>1</sup>Division of Hematology/Oncology, UPMC Children's Hospital of Pittsburgh; <sup>2</sup>Division of Medical Genetics,  
25 UPMC Children's Hospital of Pittsburgh; <sup>3</sup>Division of Endocrinology, UPMC Children's Hospital of  
26 Pittsburgh; <sup>4</sup>The Department of Microbiology and Molecular Genetics, UPMC; <sup>5</sup>The Hillman Cancer Center  
27 of UPMC; <sup>6</sup>The Pittsburgh Liver Research Center, UPMC, Pittsburgh, PA. 15224  
28

29  
30  
31 <sup>7</sup>Address correspondence to:  
32 Edward V. Prochownik, M.D., Ph.D.  
33 Division of Hematology/Oncology  
34 UPMC Children's Hospital of Pittsburgh  
35 Rangos Research Center  
36 Room 5124  
37 UPMC Children's Hospital of Pittsburgh  
38 4401 Penn Ave.  
39 Pittsburgh, PA 15224  
40 Tel: (412)-692-6795  
41 Email: [procev@chp.edu](mailto:procev@chp.edu)  
42

43

44 **Abstract**

45

46 The “Mlx” and “Myc” Networks share many common gene targets. Just as Myc’s activity depends upon its  
47 heterodimerization with Max, the Mlx Network requires that the Max-like factor Mlx associate with the Myc-  
48 like factors MondoA or ChREBP. We show here that body-wide *Mlx* inactivation, like that of *Myc*, accelerates  
49 numerous aging-related phenotypes pertaining to body habitus and metabolism. The deregulation of numerous  
50 aging-related Myc target gene sets is also accelerated. Among other functions, these gene sets often regulate  
51 ribosomal and mitochondrial structure and function, genomic stability and aging. Whereas “*MycKO*” mice  
52 have an extended lifespan because of a lower cancer incidence, “*MlxKO*” mice have normal lifespans and a  
53 somewhat higher cancer incidence. Like Myc, Mlx, MondoA and ChREBP expression and that of their target  
54 genes, deteriorate with age in both mice and humans, underscoring the importance of life-long and balanced  
55 cross-talk between the two Networks to maintain normal aging.

56

57

58 **Teaser**

59

60 Inactivation of the Myc-like "Mlx Network" in mice leads to phenotypic and molecular signs of premature  
61 aging and a cancer predisposition.

62

## 63 Introduction

64

65 The bHLH-ZIP transcription factor (TF) c-Myc (Myc) is de-regulated and/or over-expressed in most human  
66 cancers, is highly transforming in various *in vivo* contexts and can be linked functionally to most canonical  
67 “Cancer Hallmarks” (1-3). Upon heterodimerizing with its bHLH-ZIP partner Max, Myc binds one or more “E  
68 box” sites (CACGTG) that usually reside in the proximal promoters of its many direct target genes. It then  
69 recruits an assortment of companion co-factors such as histone acetylases and H3K4 methylases thereby  
70 facilitating transcriptional initiation and read-through and reducing pausing by RNA pol II (4-6). These  
71 activities are countered by four tissue-restricted bHLH-ZIP “Mxd” members (Mxd1-4) or the more distantly  
72 related factors Mnt and Mga. These also heterodimerize with Max and compete with one another and with  
73 Myc-Max for E-box occupancy and negate Myc target gene activation by recruiting histone deacetylases (7, 8).  
74 Myc-Max-driven interactions are favored during rapid proliferation when Myc is highly expressed whereas  
75 Mxd/Mnt/Mga-Max interactions predominate during periods of quiescence or in differentiated cells when Myc  
76 levels are low or declining (7, 8). Negative transcriptional regulation by Myc, which accounts for nearly half of  
77 its effects on gene expression, is indirect, E-box-independent and mediated by inhibitory interactions between  
78 Myc-Max and TFs such as Miz1 and Sp1/3, which bind at their own distinct promoter-proximal Miz1 and SP1  
79 sites, respectively (9, 10).

80 Fundamental processes supervised by the above “Myc Network” include ribosomal biogenesis and  
81 translation, cell cycle progression and energy production (7, 11-14). The latter encompasses glycolysis,  
82 glutaminolysis, fatty acid oxidation (FAO), oxidative phosphorylation (Oxphos) and the maintenance of  
83 mitochondrial structure (1, 13-18). Collectively, these processes support biomass accumulation and the  
84 maintenance of a reduced intracellular environment, all of which decline with age as does the expression of  
85 Myc itself and many of its direct target genes (11, 19-24).

86 A second group of bHLH-ZIP TFs with structural and functional relatedness to Myc Network members are  
87 those which comprise the “Mlx Network” (13, 14, 25, 26). They regulate a smaller direct target gene repertoire  
88 than do Myc Network TFs although considerable overlap exists (13, 14, 24-29). The positively-acting, Myc-  
89 like members of this Network, ChREBP and MondoA, interact with the Max-like protein Mlx to form  
90 transcriptionally active heterodimers. Unlike Myc, however, their nuclear import and transcriptional activity  
91 are dependent upon their binding of glucose-6-phosphate, thus making them nutrient-responsive and  
92 subservient to metabolic cues (26). While these heterodimers recognize E boxes (13, 14, 25), they classically  
93 bind to more complex “carbohydrate response elements” (ChoREs) consisting of tandem E box-like elements  
94 separated by 5 nucleotides (13, 14, 30). This binding site flexibility is reinforced by the fact that Mxd1, Mxd4  
95 and Mnt can also heterodimerize with Mlx, displace ChREBP/MondoA-Mlx heterodimers and counter their  
96 positive effects on transcription (7, 25, 31, 32). In addition to being fewer in number, Mlx Network direct  
97 target genes were initially believed to be more functionally restricted than those of the Myc Network and were  
98 primarily viewed as participating in lipid and carbohydrate metabolism (7, 25, 31-35). More recently, however,  
99 extended roles for the Mlx Network in maintaining ribosomal and mitochondrial structure and function, both  
100 alone and in collaboration with Myc, have been reported (13, 14, 24, 28, 29).

101 The mid-gestational embryonic lethality associated with *Myc* gene inactivation has until recently stymied a  
102 complete understanding of its role(s) in normal physiology, particularly over the course of a lifetime (36). *In*  
103 *vivo* studies therefore have been restricted to examining the consequences of such inactivation in individual  
104 tissues or in *Myc*<sup>+/-</sup> mice, both of which are compatible with long-term survival (15, 37-39). *Myc*<sup>+/-</sup> animals  
105 are smaller than their WT counterparts, age less rapidly, live significantly longer and are generally healthier.  
106 These studies showed that Myc impacts aging although precisely how and the degree to which the smaller size  
107 of the animals might have contributed to this was not addressed (38, 40). They also suggested that a more  
108 complete loss of Myc would reveal additional phenotypes.

109 We recently reported the long-term consequences of near-complete body-wide *Myc* gene inactivation in  
110 mice initiated at the time of weaning (23, 40). The survival of these “*Myc*KO” mice permitted the long-term

111 consequences of the gene's loss to be studied and its impact on aging to be determined. Unlike *Myc*<sup>+/-</sup> mice,  
112 *Myc*KO mice were of normal size or even somewhat larger than their wild-type (WT), *Myc*<sup>+/+</sup> counterparts.  
113 However, they gradually developed many features of premature aging that coincided with the dysregulation of  
114 numerous gene sets involved in ribosomal and mitochondrial structure and function, oxidative stress, redox  
115 balance, mRNA splicing and DNA damage response and repair. They also prematurely altered the expression  
116 of multiple sets of genes typically associated with normal or premature aging and senescence. Yet despite their  
117 pronounced premature aging profiles, *Myc*KO mice lived significantly longer than WT mice, most likely as a  
118 result of their having a 3-4-fold lower lifetime incidence of cancer, the generation and maintenance of which is  
119 highly *Myc*-dependent (3). The infrequent tumors that did arise tended to originate from minority cell  
120 populations that had escaped complete *Myc* excision. Remarkably, normal mouse and human tissues  
121 commonly showed significant age-related declines in *Myc* expression and an even more extensive loss of  
122 properly maintained *Myc* target gene expression. Together, these findings showed that the long-known  
123 intimate association between aging and cancer could be broken and was maintained to a large degree by a  
124 single gene, namely *Myc* (23, 41).

125 Given the substantial overlap of the target genes regulated by the *Myc* and *Mlx* Networks (13, 14, 25), we  
126 sought to determine here whether and to what extent the body-wide inactivation of *Mlx* recapitulates any of the  
127 life-long consequences previously described in *Myc*<sup>+/-</sup> or *Myc*KO mice (23, 38, 40). Because the loss of *Myc*  
128 can either slow or accelerate aging in a manner than reflects gene dosage (23, 24, 40), we paid particular  
129 attention to age-related phenotypes. In doing so, we chose to *inactivate* *Mlx* in the same manner as we  
130 previously did for *Myc* (i.e. at the time of weaning) so as to ensure that any observed differences were unlikely  
131 to be attributable to the timing or extent of target gene knockout or the manner by which this was achieved.  
132 This allowed us to demonstrate that *Mlx*KO mice display some of the same whole body, tissue and molecular  
133 changes as their age-matched *Myc*KO counterparts while also manifesting distinct differences that are  
134 consistent with the interplay between the two Networks.

135

## 136 Results

137

138 Post-natal excision of the *Mlx* locus is highly efficient and permanent. *Mlx*<sup>LoxP/LoxP</sup> C57Bl6 mice containing  
139 either one or 2 copies of the ROSA-CreER transgene were generated as described previously and as  
140 summarized in Supplementary Figure 1A-D (23, 24). Control mice were the progeny of crosses between  
141 ROSA-CreER strain and C57Bl6 mice with unmodified *Mlx* loci that are hereafter referred to as “WT” (wild-  
142 type) mice. At the time of weaning and upon attaining weights of at least 15 g, all mice were subjected to 5  
143 daily injections of tamoxifen as previously described (75 mg/Kg/day i.p. in corn oil) (23) and the degree of *Mlx*  
144 gene excision was evaluated 2 weeks later. On average, excisional efficiencies were higher in mice bearing 2  
145 copies of the CreER transgene and correlated with both *Mlx* transcript and protein expression (Supplementary  
146 Figure 1E&F and Supplementary Table 1). They were therefore used in all subsequent studies and are referred  
147 to as “*Mlx*KO” mice. *Mlx* gene excision persisted throughout life and no evidence was obtained to indicate a  
148 selective expansion of cells with retained *Mlx* alleles (Supplementary Figure 1E and Supplementary Table 1).

149

150 *Mlx*KO mice show signs of accelerated aging but have normal lifespans. WT and *Mlx*KO mice of both sexes  
151 initially showed similar growth rates and maintained indistinguishable weights and fat:lean mass ratios until  
152 ~10 months of age. At this point, females diverged, gaining weight more rapidly and attaining their maximum  
153 adult weights ~4 months earlier than WT mice (~20 months vs. 24 months). Fat:lean mass ratios also peaked  
154 ~4 months earlier in female *Myc*KO mice and then subsequently declined at similar rates (Figure 1A).

155 Premature fur loss (alopecia) and graying (achomotricia) previously observed in *Myc*KO mice, and first  
156 noted at ~5-6 months of age, was not observed in *Mlx*KO mice. However, over two-thirds of the latter animals  
157 of both sexes eventually developed unilateral or bilateral corneal opacifications (leucoma simplex) compared  
158 to <20% of WT animals (Figure 1B and C). Thus, *Mlx*KO mice developed another external feature of

159 premature aging that was not seen in *Myc*KO mice.

160 Young male *Mlx*KO mice were significantly weaker than WT mice as measured by grip strength testing  
161 (23), although this improved with age such that the oldest mice were actually somewhat stronger than their  
162 age-matched WT counterparts (Figure 1D). These mice also showed a progressive deterioration in endurance  
163 when subjected to treadmill testing (Figure 1E). In contrast, female *Mlx*KO and WT mice could not be  
164 distinguished by these tests, irrespective of age. Nor were any differences in balance noted among age-matched  
165 cohorts of either sex based on Rotarod testing (Figure 1F). Finally, overall diurnal ambulatory activity,  
166 measured during the course of metabolic cage studies (see below), showed no differences until 18-20 months  
167 of age when female mice became significantly less active (Figure 1G). Collectively, the results presented in  
168 Figure 1A-G show that *Mlx*KO mice prematurely developed several mild features and behaviors associated  
169 with aging, although they were somewhat distinct from those seen in *Myc*KO mice (23).

170 The longer survival of *Myc*KO mice has been attributed in part to their >3-fold lower lifetime cancer  
171 incidence owing to the virtual absence of this important oncogenic driver (1, 3, 23, 40). In contrast *Mlx*KO  
172 mice and WT mice of both sexes demonstrated identical lifespans although *Mlx*KO mice had 1.5-fold higher  
173 incidences of lymphoma and a 1.7-fold fold higher incidence of other tumors at the time of death (Figure 1H  
174 and I). This was in keeping with previous reports that *Mlx* can function as a suppressor (23, 31, 40).

175

176 *Mlx*KO mice accumulate excessive hepatic lipid and malabsorb dietary fat. The incidence of hepatic fat  
177 accumulation (steatosis) by both mice and humans increases with age, particularly in association with obesity  
178 and insulin resistance (42, 43). *Myc*KO mice also manifest a higher incidence and earlier onset of steatosis and  
179 both the genetic and pharmacologic inhibition of *Myc* in a variety of cell types is associated with excessive  
180 neutral lipid accumulation (15, 23, 24, 28, 29, 44). Similarly, mice with hepatocyte-specific knockout of  
181 *Chrebp* or *Mlx* develop steatosis although precisely when it begins and its natural history have not been  
182 investigated (28, 29). We confirmed and extended these findings by showing that *Mlx*KO mice as young as 5  
183 months showed more intense hepatic staining with Oil Red O and accumulated ~4 times more triglyceride  
184 (Figure 2A and B). As mice aged, this disparity lessened, although it remained elevated in the latter animals  
185 throughout the duration of the study.

186 *Myc*KO mice and those with body-wide expression of the dominant negative inhibitor OmoMyc develop  
187 transient flattening of their intestinal mucosa that is not severe enough to cause malabsorption or impair growth  
188 (23, 45). In contrast, *Mlx*KO mice retained the normal architecture of both their small and large intestines but  
189 showed an increased fecal fat content that was noted as early as ~5-6 months of age and persisted for longer  
190 than 11 months (Figure 2C and D). However, as with the above-mentioned reports (23, 45) this did not impact  
191 growth (Figure 1A).

192

193 *Mlx*KO mice are overly reliant on fatty acid oxidation as an energy source while displaying metabolic  
194 inflexibility and abnormal mitochondrial function. Previous metabolic cage studies have shown *Myc*KO mice  
195 to be overly reliant on fatty acids as an energy source, particularly during nocturnal feeding when glucose  
196 availability is high and normally constitutes the primary energy-generating substrate (23). This excessive FAO  
197 dependency is also maintained during post-fasting re-feeding with either standard or high-fat diets (HFDs)  
198 (23). Two month old *Mlx*KO mice showed a similar nocturnal FAO dependency (Figure 3A). Unlike *Myc*KO  
199 mice, however, they were also more reliant on glucose during the day when feeding normally declines and  
200 fatty acids become alternative energy-generating substrates. The decreased amplitude of the diurnal fluctuation  
201 in respiratory exchange ratio (RER =  $[VCO_2/VO_2]$ ) of *Mlx*KO mice pointed to them as being “metabolically  
202 inflexible”, a condition whereby excessive nutrient overload and over-competition for metabolic substrates can  
203 cause dysregulation in fuel choice and energy generation (46). The markedly lower RERs in both WT and  
204 *Mlx*KO cohorts in response to fasting indicated that they were similarly adaptable to a period of exogenous  
205 glucose deprivation that was rectified by switching their energy source to fatty acids. However, the *Myc*KO  
206 cohort’s over-dependence on FAO persisted when either standard or HFDs were re-introduced. The metabolic  
207 disparities between *Myc*KO and WT mice changed somewhat over life such that in older adults (ca. 20 months)

208 the excessive reliance on FAO became more generalized across the entire day (Figure 3A).

209 To determine whether the exaggerated FAO dependency of *Mlx*KO mice was a consequence of Type 2  
210 diabetes (T2D)-like insulin insensitivity as previously described in *Myc*KO mice (23), glucose tolerance tests  
211 (GTTs) were conducted with age-matched WT mice serving as controls. In 2 month old mice, no inter-group  
212 differences were observed in the peak glucose levels achieved after glucose administration or in the kinetics of  
213 the initial glucose response and its normalization (Figure 3B). Nor did the two groups differ in their insulin  
214 kinetics in response to the glucose challenge. By 5 months, however, *Mlx*KO mice demonstrated higher  
215 peripheral glucose levels and delayed normalization following the glucose challenge. While mimicking the  
216 response previously seen in *Myc*KO mice (23), the underlying basis for this transient hyperglycemia was quite  
217 different. Rather than the T2D-like exaggerated and prolonged hyperinsulinemia seen in *Myc*KO mice, the  
218 insulin response of *Mlx*KO mice was blunted and more akin to that associated with Type 1 diabetes (T1D).  
219 Further metabolic profiling showed that *Mlx*KO mice were intermittently prone to the development of fasting  
220 hyperglycemia and lactic acidemia (Figure 3C-E). Together with the previous metabolic cage experiments,  
221 these studies indicate that *Mlx*KO mice increase their reliance on FAO at least in part because they secrete  
222 insufficient amounts of insulin to allow for the adequate uptake of glucose.

223 Many genes whose encoded proteins contribute to mitochondrial structure and function are co-regulated by  
224 both the *Myc* and *Mlx* Network members (13, 24, 29, 41). Given the above-noted metabolic abnormalities in  
225 *Mlx*KO mice, we examined 3 tissues (liver, skeletal muscle and abdominal white adipose tissue) in which  
226 mitochondrial function is known to be compromised by *Myc* loss and/or aging (15, 23, 24, 43, 47-49).  
227 Respirometry studies performed on liver mitochondria from 5 month old WT and *Mlx*KO mice showed  
228 attenuated responses in the latter group to non-rate-limiting amounts of all tested substrates for Complex I  
229 (malate and pyruvate), Complex II (succinate), and fatty acid oxidation (palmitoyl-coenzyme A) (Figure 4A).  
230 In contrast, no differences were seen in the responses of skeletal muscle mitochondria, whereas in white  
231 adipose tissue mitochondria, both Complex I and Complex II defects were noted with the former being  
232 confined largely to the pyruvate response (Figure 4B and C). Mitochondrial function in tissues of older mice  
233 was also similar, with the only noticeable defect being a suppressed response to palmitoyl-coenzyme A in  
234 *Mlx*KO livers (Figure 4D-F). The Complex I and Complex II defects in younger *Mlx*KO mice thus resembled  
235 those identified previously in association with aging and/or *Myc* loss in various tissues with the exception of  
236 skeletal muscle, which tended to display little, if any, age-related declines in mitochondrial function (15, 29,  
237 50, 51).

238 Serum acyl carnitine measurements can serve as surrogates for body-wide mitochondrial dysfunction and  
239 are useful for diagnosing Complex I defects (52). Mass spectrometry-based quantification of 51 serum  
240 carnitines revealed lower levels of C14:2 and C18:3 in 5 month old *Mlx*KO mice (Figure 4G and  
241 Supplementary Table 2). Rather than indicating mitochondrial dysfunction, this finding suggested a more  
242 rapid mitochondrial uptake and preferential utilization of these long-chain fatty acids for FAO as documented  
243 by metabolic cage profiling (Figure 3). The failure of these disparities to persist in older mice (Figure 4H)  
244 could indicate that the source of fatty acids changed over time, from those circulating in serum to those that  
245 had accumulated in tissues and thus were potentially more readily accessible (Figure 2A).

246 Age was more strongly associated with changes in serum acyl carnitines than was *Mlx* status and, in both  
247 cohorts, tended to reflect the loss of mitochondrial efficiency in general and Complex I specifically in older  
248 mice (Figure 4I and J and Supplementary Tables 2-5) (47, 48, 51). A tendency for age-related increases in  
249 serum dicarboxylic acids may have indicated a preferential shunting of serum fatty acids into non-energy-  
250 generating peroxisomal and lysosomal FAO pathways as seen in inborn errors of long chain fatty acid  
251 oxidation, while maintaining a reliance on tissue stores of fatty acids for mitochondrial utilization(53).

252 Compromised *Myc* and *Mlx* function can lead to structural and/or functional defects in the electron  
253 transport chain (ETC) along with altered mitochondrial size, number, ultrastructure and ATP generation (15,  
254 18, 24, 44). Blue native gel electrophoresis (BNGE) and *in situ* enzymatic evaluations of ETC Complexes I,  
255 III, and IV from WT and *Mlx*KO livers of 5 month old mice revealed no overt differences between the two

256 groups (Figure 5A). In contrast, the ATPase activity of Complex V was reduced nearly 4-fold in *Mlx*KO  
257 livers (Figure 5B). Similar studies on mitochondria from skeletal and cardiac muscle of these same animals  
258 revealed no differences thereby again indicating that the consequences of *Mlx* inactivation in mice are highly  
259 tissues-specific, as they are with *Myc* (Figure 5C-F) (23).

260 Given the marked differences in fuel preferences, glucose kinetics and ETC substrate responses of *Mlx*KO  
261 mice and previously described *Mlx*KO MEFs (Figures 2A and B and 3A and B) (24), we evaluated several  
262 tissues in 5 month old mice for the expression of relevant glucose transporters, which are known to be  
263 differentially regulated by *Myc* (17, 23, 24). We focused on ubiquitously expressed Glut1/Slc2a1, which is  
264 particularly prominent in muscle and adipose tissue; Glut 2/Slc2a2, the major glucose transporter in liver; and  
265 Glut4/Slc2a4, which is insulin responsive and abundant in skeletal and cardiac muscle and adipose tissues  
266 (54). Each transporter showed unique changes in *Mlx*KO tissues (Figure 5G). For example, Glut1 was up-  
267 regulated in *Mlx*KO skeletal muscle tissue, Glut2 was up-regulated in *Mlx*KO liver and Glut4 was up-  
268 regulated *Mlx*KO liver, skeletal muscle and heart. We also examined the expression of several rate-limiting  
269 enzymes that control glucose's fate and mitochondrial biogenesis (Figure 5H). Notably, the liver-specific  
270 isoform of phosphofructokinase, PFK-L, was unchanged in *Mlx*KO livers, whereas the muscle-specific  
271 isoform, PFK-M, was markedly down-regulated in *Mlx*KO hearts and unaltered in *Mlx*KO skeletal muscle  
272 and adipose tissue. Pyruvate dehydrogenase (PDH), which catalyzes the mitochondrial conversion of pyruvate  
273 to acetyl coenzyme A was unaltered across all tissues, irrespective of *Mlx* gene status although its activity, as  
274 judged by levels of inhibitory phosphorylation at Ser<sub>293</sub> (pPDH), was decreased in cardiac muscle (Figure  
275 5D). Peroxisome proliferator-activated receptor-gamma co-activator 1 alpha (PGC1 $\alpha$ )/PPARGC1A, a  
276 transcriptional driver of mitochondrial biogenesis (55), was highly induced in *Mlx*KO skeletal muscle.  
277 Collectively, these findings broadly implicate *Mlx*KO in tissue-specific metabolic reprogramming involving  
278 both oxidative and non-oxidative arms of energy generation, particularly via the regulation of rate-limiting  
279 steps in glucose uptake, glycolysis, FAO and mitochondrial biogenesis.

280

281 Transcriptional reprogramming of *Mlx*KO tissues involves subsets of *Myc* Network-regulated genes. *Mlx*  
282 Network members also bind to numerous *Myc* target genes (13, 14, 25, 56). Using RNA-seq, we compared  
283 the liver, abdominal adipose tissue and skeletal muscle transcriptomes from young (5 month old) and old (20  
284 month old) *Mlx*KO and WT mice. Our recent studies on these tissues from *Myc*KO mice of the same ages also  
285 allowed us to compare and contrast gene expression profiles between the two KO cohorts (23).

286 We first used Gene Set Enrichment Analysis (GSEA) to verify that a previously authenticated 282-  
287 member Chrebp/MondoA/*Mlx* target gene set from the EnrichR database and a 157-member direct target set  
288 from the Qiagen IPA collection were dysregulated as expected in all 3 tissues from young *Mlx*KO mice  
289 (Supplementary Figure 2A and B) (23). While the magnitude of this dysregulation and the identities of  
290 individual affected genes varied among the tissues, the findings validated their use for all subsequent  
291 analyses. Consistent with previous findings that some *Mlx* Network target genes are also direct *Myc* Network  
292 targets (23-25, 31, 56) many of the transcripts from the above gene sets were also altered in the corresponding  
293 tissues from 5 month old *Myc*KO mice, albeit to a somewhat lesser degree (Supplementary Figure 2C and D).  
294 These results confirmed that *Mlx* inactivation was associated with the anticipated tissue-specific changes in  
295 the expression of its target genes. They also documented significant and complex cross-talk between the *Mlx*  
296 and *Myc* Networks, with some of the genes being responsive to *Mlx* only, others to *Myc* only and others  
297 being duly responsive to both factors (13, 14, 23, 24).

298 Three unbiased analytic methods (CLC Genomics, DeSeq and EdgeR) were used to capture gene  
299 expression differences between the above age-matched *Mlx*KO and WT tissues while ensuring the highest  
300 degree of confidence in their selection. Only transcripts identified as being differentially expressed by all 3  
301 methods ( $q < 0.05$ ) were included in our final analysis. In 5 month old *Mlx*KO mice, 150 individual transcripts  
302 in livers met this criterion. Of these, 60 (40%) were previously identified as putative direct *Mlx* and/or  
303 MondoA targets based on a compilation of Chip-Seq results from 3 available human cell lines in the

304 ENCODE database (HepG2 hepatoblastoma, K562 chronic myelogenous leukemia/lymphoid blast crisis and  
305 WTC11 induced pluripotent stem cells) (57). In adipose tissue, 2163 such differences were noted, 891 of  
306 which (41.2%) were direct Mlx/MondoA targets and in skeletal muscle, only 3 differences were noted, with 2  
307 being direct targets. An initial analysis using Ingenuity Pathway Analysis (IPA) indicated that these 2316  
308 genes were most commonly involved in oxidative phosphorylation (Oxphos), translation and responses to  
309 glucose and other nutrients as we and others have previously observed (7, 13, 14, 24-26).

310 GSEA was next used to expand these findings by identifying functionally related and coordinately  
311 dysregulated gene sets. Doing so in *Myc*KO tissues had previously revealed 7 such major categories, each  
312 comprised of multiple gene sets involved in ribosomal and mitochondrial structure and function, DNA  
313 damage response/repair, oxidative stress response, aging, senescence and mRNA splicing (23, 24). These  
314 categories were also identified in *Mlx*KO tissues, albeit with a different collection of gene sets and enrichment  
315 scores (Figure 6A, Supplementary Figures 3-9 and Supplementary File 1). A notable finding in the “DNA  
316 damage response/repair” category was that the enriched gene sets in *Mlx*KO tissues tended to be more  
317 restricted to those involving the recognition and repair of UV radiation-induced DNA damage whereas  
318 enriched gene sets in *Myc*KO tissues were more diverse, involving the repair of base-pair mis-matches, inter-  
319 and intra-strand cross-links, single- and double-stranded DNA breaks and shortened telomeres (23, 24).

320 In addition to the above categories that were shared with *Myc*KO tissues, we identified 6 others that were  
321 more prominent in or unique to *Mlx*KO tissues. The gene sets comprising them encoded miRNA targets or  
322 proteins participating in glycolysis, lipid metabolism, Wnt/ $\beta$ -catenin/Tcf signaling, Hippo/YAP/TAZ  
323 signaling and chromatin/histone modification (Figure 6B and Supplementary Figures 10-15 and  
324 Supplementary File 2).

325 GSEA from the above tissues of *Myc*KO mice had previously revealed the suppression of numerous gene  
326 sets that are often collectively up-regulated in various cancers (23). Because many of the individual genes  
327 comprising these sets were also direct *Myc* targets, this finding was consistent with the 3.4-fold lower lifetime  
328 cancer incidence we have reported for these animals (23). In contrast, 5 month old *Mlx*KO mice tended to  
329 show an up-regulation of these gene sets (Figure 6C, Supplementary Figures 16 and 17 and Supplementary  
330 File 3). Overall, these results were in agreement with previously proposed contrasting roles for Mlx in tumor  
331 suppression versus *Myc*'s role in tumor promotion (7, 13, 14, 23, 24, 26).

332 An additional category of gene sets previously identified as being enriched in *Myc*KO tissues was  
333 comprised of those that associated with either T2D or T1D and was consistent with the T2D-like GTTs and  
334 insulin kinetics of these animals (23). Conforming to the T1D-like profiles of *Mlx*KO mice (Figure 3B and  
335 C), this category of gene sets was dysregulated although the precise identities of the gene sets again differed  
336 from those of *Myc*KO mice (Figure 6D and Supplementary Figures 18 and 19 and Supplementary File 4).

337 We next asked how gene expression profiles differed among tissues from 5 month old and 20 month old  
338 *Mlx*KO mice. To ensure that these results were again compiled in an unbiased and comprehensive manner, we  
339 searched the MSigDB and Enrichr databases for gene sets comprising each of the functional categories shown  
340 in Figure 6A-D as well as for novel categories of gene sets (Supplementary File 2). This broader search  
341 confirmed the overall directionality of the selected gene sets depicted in Figure 6A-D while revealing as many  
342 as 1957 additional gene sets in the “miRNA target” category to as few as 18 in the “Senescence” category  
343 (Figure 6E-column 1 and Supplementary File 5). In tissues of 20 month old WT and *Mlx*KO mice, a smaller  
344 total number of these enriched gene sets was noted and, in some cases, the direction of the dysregulation was  
345 the opposite of that seen at 5 months (Figure 6E-column 2). Comparing the gene sets of 5 month old and 20  
346 month old mice showed many of the above gene sets to be both age- and Mlx-dependent (Figure 6E-columns  
347 3 and 4).

348 We also determined whether tissues from 20 month WT and *Mlx*KO mice differed in the enrichment of  
349 functionally related gene sets that were either not detected during the initial analysis of 5 month old tissues or  
350 that comprised minor categories. Doing so identified 3191 dysregulated gene sets across all 3 *Mlx*KO tissues  
351 related to the immune response, inflammation and the production of or response to various

352 inflammation/immune-related cytokines such as interferon gamma (IFN $\gamma$ ), tumor necrosis factor alpha  
353 (TNF $\gamma$ ), and interleukin-6 (IL-6) (Figure 6F and Supplementary File 6). These gene sets were enriched in  
354 highly tissue-specific patterns and were most prominent in liver where 1993 (62.5%) of them were  
355 significantly enriched. This was followed by adipose tissue and skeletal muscle where 999 (31.3%) and 649  
356 (20.3%) of the sets were enriched, respectively. These were readily detectable by 5 month of age but were  
357 particularly pronounced in older *Mlx*KO mice, most notably in liver and adipose tissue (Figure 6F-column 4).

358 The above results did not distinguish between direct *Mlx*-dependent transcriptional targets and secondary  
359 ones whose dysregulation was a consequence of the metabolic dysfunction-associated steatotic liver disease  
360 (MASLD) associated with *Mlx*KO mice (Figure 2) (58, 59). We therefore asked whether any of the gene sets  
361 shown in Figure 6F were also enriched in tissues of otherwise normal mice maintained on HFDs. From the  
362 GEO database and our own previous study (60), we retrieved 12 sets of RNAseq results from livers of normal  
363 mice of various strains maintained on standard or HFDs, the latter of which varied in their composition (long-  
364 chain vs. medium chain) and/or duration (10-24 weeks). Four additional HFD data sets were analyzed in  
365 adipose deposits obtained from different anatomical locations and one HFD data set was obtained from  
366 skeletal muscle. Many of the differentially enriched gene sets in these tissues and *Mlx*KO tissues were  
367 identical, thereby indicating that the immune-related transcript differences of the latter were attributable to  
368 their higher neutral lipid content and/or its associated systemic pro-inflammatory state (Figure 6G and  
369 Supplementary File 6). Comparing these gene set profiles from older *Mlx*KO mice and *Myc*KO mice, both of  
370 which accumulated comparable degrees of hepatic lipid (15, 29), continued to show differences, most notably  
371 in liver. Collectively, this analysis, which sought to equalize the contributions made by HFDs, steatosis and  
372 system inflammation, indicated that, while a majority of immune-related gene expression differences in  
373 *Mlx*KO mice were attributable to these features, other differences were specifically related to the loss of *Mlx*.

374 Relative to control mice maintained on standard diets, those on HFDs showed no significant changes in  
375 liver- or adipose tissue-associated MondoA transcript levels whereas ChREBP and *Mlx* transcripts were  
376 significantly lower (Figure 6H). Together with our previous findings that mice with hepatocyte-specific loss  
377 of ChREBP also develop MASLD in the absence of obesity, these results suggest that the lipid accumulation  
378 seen in response to HFDs requires the down-regulation of ChREBP and/or *Mlx*, which play important roles in  
379 lipid and carbohydrate metabolism (7, 13, 14, 26, 27, 32, 34, 56).

380 *Myc* expression normally declines with age in a number of murine and human tissues (23). To determine  
381 whether this also occurs with any of the above *Mlx* Network members, we compared RNA-seq results from  
382 90 single cell (sc) populations originating from 23 tissues from young (1-3 months) and old (18-30 months)  
383 mice (Figure 6I) (61). Significant age-related declines were noted in MondoA transcripts in 16 sc populations,  
384 declines in ChREBP transcripts were noted in 2 sc populations, and declines in *Mlx* transcripts were noted in  
385 8 sc populations. Examination of total organ transcripts from young and old humans (ages 20-49 and 60-79,  
386 respectively) from the Broad Institute's GTEx database (<https://gtexportal.org/home/>) also showed age-related  
387 declines in MondoA, ChREBP and *Mlx* expression in several tissues as well as in *in vitro* cultured primary  
388 skin fibroblasts (Figure 6J) (62). Thus, like *Myc* transcripts (23, 40), those of some *Mlx* Network members  
389 progressively decline in some normal aging tissues. In this setting, the co-regulation of many *Myc* target  
390 genes by *Mlx* Network members may explain why the previously observed loss of regulation of *Myc* target  
391 genes in response to aging was often more pronounced than was the decline of *Myc* itself (23).

392

## 393 DISCUSSION

394

395 The *Mlx* Network target gene repertoire, originally thought to regulate glucose and lipid metabolism, has  
396 recently been expanded to include the maintenance of mitochondrial structure and function, ribosomal  
397 biogenesis and translation and other functions described here and elsewhere (Figure 6A-E) (7, 14, 26, 32, 34,  
398 40, 56, 63). Numerous Chip-seq results have demonstrated that *Myc* and *Mlx* Network members can compete  
399 for the same E box and/or ChoREs in positively-regulated target gene promoters or bind to distinct elements

400 in close physical proximity, with similar co-regulation extending to negatively-regulated target genes (23, 24,  
401 40, 57, 63). Indeed, the loss of *Mlx* Network members may in some cases have a greater impact on the  
402 expression of previously identified direct *Myc* target genes than does the loss of *Myc* itself and *vice versa* (23,  
403 24, 28). For these reasons, and because the target gene sets regulated by these two Networks are not identical,  
404 it is perhaps unsurprising that premature aging would be observed in *Mlx*KO mice with the individual  
405 phenotypes overlapping those described in *Myc*KO mice (23).

406 *Mlx*KO females achieved their maximal body weights earlier than WT mice while also attaining a higher  
407 fat:lean mass ratio although this was not nearly as pronounced as that seen in *Myc*KO mice (Figure 1A) (23).  
408 The fat content and body mass of these individuals also began their declines earlier than they did in WT mice.  
409 Although *Mlx*KO mice did not manifest the premature alopecia or achromotricia that typifies *Myc*KO mice,  
410 they did accumulate an overall ~3-fold higher lifetime incidence of corneal opacities than either WT mice or  
411 *Myc*KO mice (Figure 1C) (23). Male *Mlx*KO mice also had less endurance when subjected to treadmill testing  
412 and both sexes showed reduced diurnal ambulatory activity, although this was again more prominent in  
413 females (Figure 1E and G). Together these findings show that *Mlx*KO and *Myc*KO mice develop both  
414 common and unique features that are consistent with premature aging.

415 Despite their various co-morbidities that would be expected to reduce lifespan, *Myc*KO mice actually live  
416 up to 20% longer than WT mice (23). We have attributed this to their 3.4-fold lower lifetime incidence of  
417 cancer, which is the major associated finding at the time of death in most inbred mouse strains and which  
418 often requires *Myc* to initiate and/or maximize neoplastic growth (1, 13, 14, 45, 64). In contrast, *Mlx*KO mice  
419 of both sexes had the same lifespans as WT mice despite a ~1.5-1.7-fold higher cancer incidence (Figure 1H  
420 and I). This is consistent with previous observations that *Mlx* is a suppressor of both normal and neoplastic  
421 cell growth, as are other *Mlx* and *Myc* Network members such as *Mxd1*, *Mxd4* or *Mnt* (13, 14, 25, 65-67).  
422 Thus, unlike *Myc*KO mice in which aging and cancer development can be dissociated so as to increase  
423 longevity, *Mlx*KO mice retain this link or even strengthen it, due presumably to both the retention of *Myc* and  
424 the loss of competition from the *Mlx* Network.

425 The increased fecal fat content of *Mlx*KO mice (Figure 2D) has not been previously observed in either WT  
426 or *Myc*KO mice at any age (23). Fat malabsorption in aging humans is common and is often caused by  
427 imbalances in the intestinal flora or other factors that alter the uptake of monoglycerides and fatty acids by  
428 intestinal enterocytes (68). Our inability to discern any consistent histologic changes in either the small or  
429 large intestines of *Mlx*KO mice (Figure 2C) indicates that these are unlikely to be causes of their steatorrhea,  
430 particularly since we have not observed it in *Myc*KO mice in which more pronounced structural defects of  
431 their intestinal vili are observed, albeit transiently following the loss of *Myc* (23, 45). Other non-mutually  
432 exclusive possibilities to explain our finding include an inability to synthesize or excrete bile acids and  
433 pancreatic exocrine insufficiency. Regardless of the cause, the observed malabsorption was not significant  
434 enough to impair normal growth (Figure 1A).

435 In both mice and humans, the incidence of MASLD normally increases with age and is exacerbated by  
436 resistance to or under-production of insulin, both of which force a switch from glucose to fatty acids as the  
437 preferred energy-generating substrate (42, 43). Age-related declines in *Myc* and mitochondrial efficiency may  
438 be at least partially responsible for this switch and the resulting lipid accumulation that exceeds the amount  
439 needed to generate sufficient energy (15, 47, 50, 51, 69-71). Normal and neoplastic tissues of non-hepatic  
440 origin are also driven to accumulate neutral lipid following the genetic or pharmacologic compromise of *Myc*  
441 (44). That MASLD also develops in response to the knockout of *Chrebp* or *Mlx* has been attributed to a  
442 similar deregulation of many of the same *Myc* target genes that support mitochondrial integrity (13, 14, 24,  
443 25, 29). In either case, the greater dependency on FAO as a more efficient means of energy generation may be  
444 accompanied by other compensatory changes such as increases in mitochondrial mass (48, 70, 71). Changes  
445 in circulating acyl carnitines and the selective utilization of fatty acids of different lengths likely reflect the  
446 integration of normal age-related changes, those arising as a consequence of *Mlx*'s absence, and whether the  
447 lipid used for FAO derives directly from immediately available dietary sources or pre-existing tissue depots

448 (Figure 4I and J and Supplementary Table 2-5) (23).

449 Disparities in mitochondrial function and fuel selection between WT and *Mlx*KO mice were observed  
450 quite early and were reflected in RERs measured during metabolic cage studies (Figure 3A). As with *Myc*KO  
451 mice (23), this was manifested by a significantly greater reliance on FAO, particularly at night when feeding  
452 activity peaks and should provide sufficient glucose for it to be the fuel of choice. Whereas this fatty acid  
453 preference was somewhat age-dependent and erratic, a more consistent indicator of it was seen following  
454 overnight fasting when re-feeding either normal or HFDs was invariably associated with markedly lower  
455 RERs. While this reliance on FAO might have been partially attributable to the mild T1D-like responses of  
456 older animals following a glucose challenge, it did not explain the findings in younger mice who had normal  
457 GTTs and plasma insulin responses (Figure 3B and E). Thus, the abnormal RERs seen throughout life likely  
458 reflect both defects in mitochondrial function as well as the later development of inadequate insulin  
459 production. Another similarity between *Mlx*KO and *Myc*KO mice was seen in the youngest individuals (2  
460 months of age) in which nocturnal RERs never exceeded 1 as they did in WT mice (Figure 3A). When not  
461 attributable to re-feeding, RERs >1 are a reliable indicator of the high rates of fatty acid synthesis and glucose  
462 utilization that are generally associated with rapid post-natal growth and which should be blunted in response  
463 to the functional inactivation of both MondoA and ChREBP that accompanies *Mlx* KO (20, 26). The failure  
464 to note this exaggerated RER in 2 month old *Mlx*KO mice might have indicated that it was offset by their  
465 excessive reliance on FAO and/or inefficient fatty acid synthesis (26). It may also have been a result of the  
466 premature aging of these mice such that this normally transient response had already disappeared by 2 months  
467 of age. The inability of *Mlx*KO RERs to ever exceed 1 during times of post-fasting re-feeding where this  
468 response was maintained in all but the oldest WT mice, suggested that the primary cause was the high levels  
469 of FAO.

470 GSEA of *Mlx*KO tissues revealed alterations in functionally related gene sets that were consistent with the  
471 described phenotypes and behaviors (Figure 6E). Not unexpectedly some of these were also enriched in  
472 *Myc*KO tissues and MEFs and *Chrebp*KO livers (23, 24, 28). The most highly enriched gene sets within the  
473 “DNA Damage Response/Repair” category in *Mlx*KO tissues involved UV-induced DNA damage whereas  
474 those pertaining to other forms of DNA damage were less highly enriched than they were in *Myc*KO tissues  
475 and MEFs (Figure 6E and Supplementary Figure 5). This was consistent with previous observations  
476 concerning the differential sensitivities of WT, *Myc*KO and *Mlx*KO MEFs to agents that induce different  
477 types of DNA damage (24). In these studies *Myc*KO MEFs were highly resistant to virtually all forms of  
478 DNA damage whereas in *Mlx*KO MEFs, the resistance was both less pronounced and more restricted to that  
479 involving the anti-metabolite 6-thioguanine and the DNA adduct-forming agent cis-platinum. The seemingly  
480 paradoxical chemo-resistance of *Myc*KO MEFs, in contrast to the marked sensitivities of cells with  
481 monogenic defects in DNA damage recognition/repair pathways, was attributed to the much more global  
482 dysregulation of these numerous pathways, their failure to cross-talk with one another and to communicate  
483 effectively with downstream apoptotic effector pathways (23).

484 Another category of gene sets deserving of mention was a large one pertaining to “Cancer” (Figure 6C,  
485 Supplementary Figure 16-17 and Supplementary File 3). In *Myc*KO tissues, these tended to be regulated in  
486 directions opposite to those in tumors whereas in *Mlx*KO tissues, they were regulated in the same direction  
487 (23). Both findings were in keeping with the 3.4-fold lower lifetime cancer incidence of the former group of  
488 mice and the 1.5-1.7-fold *higher* cancer incidence of the latter and with the *Mlx* Network’s putative role in  
489 tumor suppression (23, 40, 65-67). The altered transcriptomic landscapes of *Mlx*KO mice implies that they  
490 might be poised for cancer development by virtue of dysregulating important cancer-related genes (including  
491 *Myc* itself) and the probable need to acquire fewer subsequent oncogenic “hits” as a result (Figure 1I).

492 We recently identified age-related declines in *Myc* expression and an even more pronounced loss of *Myc*  
493 target gene regulation in numerous murine and human tissues and have suggested that they may be directly  
494 responsible for at least some aspects of normal aging (23, 40). This notion largely derives from the fact that  
495 *Myc* oversees many critical functions that deteriorate in response to and even drive aging including DNA

496 replication, mitochondrial and ribosomal structure and function, protection against reactive oxygen species,  
497 DNA damage recognition and repair, rRNA splicing and the maintenance of proper metabolic balance  
498 (Figures 5 and 6A) (17, 19, 23, 24, 42, 43, 48, 72-74). By analogy, various combinations of *Mlx*, *MondoA*  
499 and *ChREBP* transcripts show similar age-related and tissue-specific declines in their expression (Figure 6H-  
500 J). Given that, at least in fibroblasts, over 60% of *Mlx*-responsive genes are also *Myc*-regulated (24), it is not  
501 surprising that many of the same cellular functions are affected by body-wide loss *Mlx* leading to similar  
502 premature aging phenotypes as well as others that reflect the specificities of each Network's functions.

503

## 504 **Materials and Methods**

505

506 Mouse maintenance, breeding and body-wide deletion of the *Mlx* locus. All care, breeding, husbandry and  
507 procedures were approved by The University of Pittsburgh Department of Laboratory and Animal Resources  
508 (DLAR) and the Institutional Animal Care and Use Committee (IACUC). Unless stated otherwise, mice were  
509 maintained on standard animal chow diets and water, both provided *ad libitum*. C57Bl6 mice with LoxP sites  
510 flanking exons 3 and 6 of the *Mlx* locus were a generous gift of Dr. R.N. Eisenman (Supplementary Figure  
511 1A-C)(24). They were crossed with the B6.129-*Gt(ROSA)26Sortm1(cre/ERT2)Tyj/J* strain (Jackson Labs. Bar  
512 Harbor, ME), which expresses the Cre recombinase-estrogen receptor (CreER) fusion transgene driven by the  
513 ubiquitously-expressed ROSA26 promoter (23, 24). At the time of weaning and upon reaching a weight of at  
514 least 15 g (~4 wks of age), mice containing either one or 2 copies of the CreER transgene were subjected to  
515 daily i.p. injections of tamoxifen (75 mg/Kg) in mineral oil for 5 days as previously described (23). Two wks  
516 later, randomly chosen animals from each group were selected and tissues were examined to determine the  
517 efficiency and tissue distribution of *Mlx* locus excision (Supplementary Figure 1E). Subsequent evaluations  
518 were performed throughout life to ensure the maintenance of the knockout state (Supplementary Table 1).  
519 Tamoxifen-treated offspring of *Mlx*<sup>fl/fl</sup> or *Myc*<sup>fl/fl</sup> (23) mice with intact *Mlx* and *Myc* genes served as wild-  
520 type (WT) controls.

521

522 Body fat and lean mass determinations. Beginning at the time of weaning, body weights were determined  
523 weekly until the age of 4-5 months and then every 2-3 weeks thereafter. In parallel with these studies, the  
524 fractional lean and fat content were determined using an Echo-MRI<sup>TM</sup> scanner (EMR-055, version 160301,  
525 Echo Medical Systems, Inc. Houston, TX) as previously described (23).

526

527 Strength, balance and endurance testing. A Grip Strength Meter (Harvard Apparatus, Holliston, MA) was  
528 used to assess strength at various ages as described previously (23). Balance was measured using a Rotarod  
529 apparatus (SPW Industrial, Laguna Hills, CA) and a modification of the procedure provided by Jackson  
530 Laboratories (Bar Harbor, ME) as described previously (23). Treadmill endurance was followed with a  
531 Columbus Instruments Exer 3/6 apparatus (Columbus, OH) as described previously (23).

532

533 Glucose tolerance tests (GTT) and serum glucose, lactate and ketone quantification. These studies were  
534 performed as previously described (23). For GTTs, mice were fasted for 5 hour and then injected i.p. with 2g  
535 of dextrose/kg body mass. Serum insulin levels were quantified with an Ultra Sensitive Mouse Insulin ELISA  
536 Kit (Crystal Chem, Elk Grove Village, IL). Whole blood glucose lactate and ketone levels were also  
537 measured in fasted mice (Glucose AimStrip Plus, Germaine Laboratories, Inc. San Antonio, TX; Lactate Plus  
538 Analyzer, Sports Resource Group, Inc., Hawthorne NY; Keto-Mojo Ketone Meter, Keto-Check, Inc. Napa,  
539 CA).

540

541 Mitochondrial respirometry. Oxygen consumption rates (OCRs) were determine on ~50 mg of disrupted  
542 tissue immediately after sacrifice using an Oroboros Oxygraph 2k instrument (Oroboros Instruments, Inc.,  
543 Innsbruck, Austria) as described elsewhere (23, 29, 60). Baseline OCR values were determined in 2 mL of

544 Mir05 buffer following the addition of non-rate-limiting concentrations of cytochrome c (final  
545 concentration=10  $\mu$ M), malate (2 mM), ADP (5 mM), pyruvate (5 mM), glutamate (10 mM) and palmitoyl-  
546 coenzyme A (3  $\mu$ M). Collectively, these provided an estimate of the Complex I activity whereas the addition  
547 of succinate (10 mM final concentration) provided an estimate of Complex II (succinate dehydrogenase)  
548 activity. Rotenone (0.5  $\mu$ M final concentration) was used to inhibit Complex I and to calculate the  
549 proportional contributions of Complexes I and II. To measure  $\beta$ -FAO, reactions were primed with ADP (5  
550 mM) and malate (5 mM) and then supplemented with palmitoyl-CoA (3  $\mu$ M) and L-carnitine (10  $\mu$ M).  
551 Activities were normalized to total protein.

552

553 Blue native gel electrophoresis (BNGE) and *in situ* enzymatic assays of ETC complexes and ATP synthase.

554 These evaluations were performed as described previously (15, 18). Briefly, 50-100 mg of fresh liver was  
555 placed into 0.5 ml of an ice-cold solution containing 25 mM Tris-HCl, pH 7.5; 100 mM KCl; 0.4 M sucrose  
556 and supplemented with protease inhibitor cocktail (Sigma-Aldrich, Inc. St. Louis, MO). Tissues were then  
557 disrupted by homogenization (Isobiotec, Heidelberg, Germany) followed by centrifugation at 500  $\times$  g for 10  
558 min at 4°C. The mitochondria-rich supernatant was further centrifuged at 14,000 $\times$  g for 15 min. The pellet  
559 was washed twice with the above buffer and then re-suspended at a final protein concentration of 5 mg/ml. 8  
560 mg of the suspension was disrupted with digitonin (MP Biomedicals, Solon OH) so as to provide a final ratio  
561 of protein:digitonin of 1:8 (15, 18). After incubating on ice for 20 min, Coomassie blue (5% Coomassie blue  
562 G250 in 750 mM 6-aminocaproic acid) was added (1/20 v/v), and the mixture was clarified by centrifugation  
563 at 14,000  $\times$  g for 20 min at 4°C. The supernatant was then electrophoresed on a 3-12% Native PAGE Novex  
564 Bis-Tris gel (Invitrogen, Inc. Waltham, MA) at 80 V for 4 hours at 4°C in the supplier's buffer. Gels were  
565 then stained with Bio-Safe Coomassie G250 (Bio-Rad, Hercules, CA) for 30 min and exhaustively de-stained  
566 with water. Scanning and analysis for band densities were performed using an AlphaEaseFC 2200 scanner  
567 and AlphaEaseFC software. To quantify Complex I activity (NADH ubiquinone oxidoreductase), gels were  
568 incubated in 3–4 ml of 2 mM Tris-HCl, pH 7.4; 2.5 mg/ml nitrotertrazolinum blue chloride and 0.1 mg/ml  
569 NADH at 37°C for 1–2 hours before quantifying band intensities by densitometric analysis. An average value  
570 from 3-4 gels was calculated. Complex III (CIII) (decylubiquinol cytochrome c oxidoreductase) activity was  
571 assayed by incubating gels with CIII assay solution overnight with mild agitation (18, 23). Complex IV (CIV)  
572 (cytochrome c oxidase) activity was measured by incubating the gel in 1 nM catalase, 10 mg cytochrome c  
573 and 750 mg sucrose in CIII assay buffer with mild agitation for 30 min followed by a final overnight wash in  
574 water. Complex V was quantified by measuring ATPase activity. Gels were incubated in 3–4 ml of 34 mM  
575 Tris-glycine, pH 7.8; 14 mM MgSO<sub>4</sub>; 0.2% Pb(NO<sub>3</sub>)<sub>2</sub> and 8 mM ATP for at least 3 hours at 37°C with any  
576 further incubation being performed at room temperature to further strengthen band intensities.

577 SDS-polyacrylamide gel electrophoresis (SDS-PAGE) and immunoblotting. After sacrifice, tissues were  
578 removed from WT and *Mlx*KO mice, immediately placed on ice and then divided into small sections. They  
579 were then snap-frozen in liquid nitrogen and transferred to a -80C freezer for subsequent storage. For SDS-  
580 PAGE, frozen tissue fragments were disrupted in protease inhibitor-containing SDS-PAGE loading buffer  
581 with Bullet Blender as previously described (23). Protein concentrations were measured with the Pierce™  
582 BCA Protein Assay Kit (23227, Thermo Fisher Scientific). Electrophoresis, blotting to PVDF membranes and  
583 protein detection was performed as previously described (23). Antibodies used for the detection of specific  
584 proteins were used largely to the directions of the suppliers and are shown in Supplementary Table 6.

585 Oil Red O (ORO) staining and triglyceride content of liver samples. The neutral lipid content of livers was  
586 determined as previously described (23). Briefly ORO-stained liver sections were viewed with a Leica  
587 DFC7000T microscope and overlapping images were joined using the stitching plugin program of FIJI  
588 software (23). Color de-convolution (75) was also performed in FIJI where the colors were specified in advance  
589 from ROIs respectively corresponding to strongly stained and unstained tissue and background. Oil-Red-O  
590 quantification was performed as previously described (23). Tissue triglyceride assays were performed as

591 previously described using a Triglyceride Quantification Colorimetric/Fluorimetric Kit (Cat. no. MAK266  
592 Sigma-Aldrich, Inc.) (23).

593

594 Measurement of fecal fat. Mice were individually caged and provided with standard chow diets containing  
595 4.5% fat (Picolab 5053; LabDiet, St. Louis, MO, USA). Following a 24 hr period of acclimation, feces were  
596 collected over the course of the next 48-72 hours, combined, and stored at -20C until processing.  
597 Approximately 200 mg of dried sample was re-suspended in 1 ml of PBS. Total lipids were then extracted  
598 using chloroform:methanol, dried and quantified as described after adjusting to the original weight of the  
599 sample (76).

600

601 Metabolic cage profiling and determination of respiratory exchange ratios (RERs). These studies were  
602 performed as described previously (23). Briefly, approximately 12 mice from each group, comprised of equal  
603 numbers of both sexes, were maintained individually in metabolic cages (Columbus Instruments, Inc.  
604 Columbus, OH) while being provided *ad lib* access to water and the standard mouse chow containing 5% fat  
605 described above but in powdered form. After a 48 hr acclimation period, VO<sub>2</sub> and VCO<sub>2</sub> were recorded every  
606 20 min over the ensuing 48 hr period as were food and water intake and total activity. At the conclusion of  
607 these measurements, mice were fasted overnight (12 hr) and then provided with a standard diet for 24 hr  
608 followed by a HFD (45%) for an additional 24 hr while again monitoring RERs. Data analyses were performed  
609 with the CalR Analysis online software package (<https://calrapp.org/>) (77).

610

611 Nucleic acid isolation, qPCR and qRT-PCR procedures. Tissue DNAs and RNAs were purified using DNeasy  
612 and RNeasy tissue extraction kits, respectively, according to the protocols supplied by the vendor (Qiagen,  
613 Inc., Germantown, MD). Sample quantification and purity were determined using a NanoDrop Microvolume  
614 Spectrophotometer (Thermo Fisher Scientific, Pittsburgh, PA). A quantitative TaqMan-based qPCR assay to  
615 determine the efficiency of *Mlx* locus inactivation was performed using the strategy described in  
616 Supplementary Figure 1A-D. A TaqMan-based qRT-PCR strategy was also employed to quantify the ratio of  
617 exon 1 transcripts to exon 6 transcripts in WT and *Mlx*KO tissues and to further confirm the extent of *Mlx*  
618 locus inactivation (Supplementary Figure 1E). Reverse transcription was performed using a SuperScript IV 1<sup>st</sup>  
619 Strand cDNA Synthesis Kit (Life Technologies, Inc.) under the conditions recommended by the vendor. All  
620 oligonucleotide primers and probes were synthesized by IDT, Inc. (Coralville, IA) based on sequences  
621 obtained from the *Mlx* GenBank DNA sequence: NC\_000077.7 (100977538..100983033) (Supplementary  
622 Figure 1D). All PCR and RT-PCR reactions were performed on a CFX96 Touch<sup>TM</sup> real-time PCR detection  
623 system (Bio-Rad Laboratories, Inc. Hercules, CA).

624

625 RNAseq and transcriptomic analyses. RNAseq and transcriptomic analyses were conducted on liver, skeletal  
626 muscle, and abdominal white adipose tissue RNAs obtained from WT and *Mlx*KO mice of specified ages (5  
627 per group). Total RNA purification was performed simultaneously for all samples using the QIAGEN RNeasy  
628 Mini Kit (QIAGEN, GmbH, Hilden, Germany), followed by DNase digestion utilizing the TURBO DNA-  
629 free<sup>TM</sup> Kit (Thermo Fisher Scientific Inc.) (23, 29, 60). RIN values were assessed using an Agilent 2100  
630 Bioanalyzer (Agilent Technologies, Santa Clara, CA), and samples with RIN values  $\geq 8.5$  were selected for  
631 further processing. The sequencing procedures were carried out on a NovaSeq 600 instrument by Novogene,  
632 Inc. as previously described (1, 23, 29, 60), and the raw data were deposited in the National Center for  
633 Biotechnology Information (NCBI) Gene Expression database under the accession number GSE248073. This  
634 data is accessible through the Gene Expression Omnibus (GEO).

635 Differentially expressed transcripts were identified using three methods: CLC Genomic Workbench  
636 version 23.0 (QIAGEN), EdgeR, and DeSeq2, as previously described (23, 24). For the latter two methods,  
637 raw reads from FASTQ files were mapped against the GRCm38.p6 mouse reference genome using nf-  
638 core/rnaseq v3.12.0. FeatureCounts from this analysis served as input for EdgeR and DeSeq2 analyses.

639 Ingenuity Profiling Analysis (IPA) was utilized for classifying transcripts into pathways, with significance  
640 adjusted for false discovery using the Bonferroni–Hochberg correction. Gene Set Enrichment Analysis  
641 (GSEA) was employed to detect alterations in the collective expression of functionally-related sets of  
642 transcripts. This analysis was performed using the clusterProfiler package in R. These gene sets were obtained  
643 from the Enrichr Database (<https://maayanlab.cloud/Enrichr/#libraries>) and the Molecular Signatures  
644 Database (MSigDB) v.7.2 (<http://www.gsea-msigdb.org/gsea/msigdb/index.jsp>). Heatmaps were generated  
645 using the ComplexHeatmap R package. Additionally, RNAseq results obtained from liver, skeletal muscle,  
646 and adipose tissues of 5-month-old and 20-month-old MycKO mice were extracted from previously published  
647 work and are accessible through the GEO accession number GSE223676  
648 (<https://www.ncbi.nlm.nih.gov/geo/query/acc.cgi?acc=GSE223676>) (23).

649

650 Bioinformatics analyses and database searches. The mouse single-cell RNAseq data used to assess the  
651 expression of Mlx, MondoA (Mlxip), and ChREBP (Mlxipl) were obtained from  
652 <https://figshare.com/ndownloader/files/27856758>. These data were analyzed for gene and aging correlations  
653 (78). The aging correlation of Mlx, MondoA (Mlxip), and ChREBP (Mlxipl) was examined across various  
654 tissue cells. Significant tissues were identified and visualized using ggplot2.

655 Transcript levels for Mlx, MondoA (Mlxip), and ChREBP (Mlxipl) in tissues from young and elderly  
656 humans were collected from the GTEx Portal (GTEx Analysis V8 release: RNAseq gene TPMs by tissue) at  
657 <https://gtexportal.org/home/datasets> (dbGaP: phs000424.v8.p2).

658 Additionally, RNA-seq datasets for normal mice of different strains, maintained on either standard or high-  
659 fat diets (HFDs), were downloaded from GEO databases. Detailed information is available in Supplementary  
660 file 7. Signal-to-noise rank lists were generated from the normalized transcription levels using GSEA v4.3.2  
661 (79) for gene set enrichment analysis.

662

663 Statistical analyses. All statistical analysis used GraphPad Prism v9.00 (GraphPad Software Inc., USA) and R  
664 software v4.2.0 (R Foundation for Statistical Computing, Vienna, Austria) as previously described (23).  
665 ggplot2 and ComplexHeatmap packages were used for boxplot and heatmap visualizations and the survminer  
666 package was used to plot survival curves. A 2-tailed, unpaired t-test was used to assess significant differences  
667 between normally distributed populations, and a 2-tailed Mann-Whitney exact test was used for the analysis  
668 of non-normally distributed populations.

669

670

## 671 **References**

672

- 673 1. J. M. Dolezal *et al.*, Sequential adaptive changes in a c-Myc-driven model of hepatocellular  
674 carcinoma. *J Biol Chem* **292**, 10068-10086 (2017).
- 675 2. D. Hanahan, R. A. Weinberg, Hallmarks of cancer: the next generation. *Cell* **144**, 646-674 (2011).
- 676 3. M. Kalkat *et al.*, MYC Deregulation in Primary Human Cancers. *Genes (Basel)* **8**, (2017).
- 677 4. M. Kalkat *et al.*, MYC Protein Interactome Profiling Reveals Functionally Distinct Regions that  
678 Cooperate to Drive Tumorigenesis. *Mol Cell* **72**, 836-848 e837 (2018).
- 679 5. C. H. Lin, C. Lin, H. Tanaka, M. L. Fero, R. N. Eisenman, Gene regulation and epigenetic  
680 remodeling in murine embryonic stem cells by c-Myc. *PLoS One* **4**, e7839 (2009).
- 681 6. W. B. Tu *et al.*, MYC Interacts with the G9a Histone Methyltransferase to Drive Transcriptional  
682 Repression and Tumorigenesis. *Cancer Cell* **34**, 579-595 e578 (2018).
- 683 7. P. A. Carroll, B. W. Freie, H. Mathsyaraja, R. N. Eisenman, The MYC transcription factor network:  
684 balancing metabolism, proliferation and oncogenesis. *Front Med* **12**, 412-425 (2018).
- 685 8. G. A. McArthur *et al.*, The Mad protein family links transcriptional repression to cell  
686 differentiation. *Cold Spring Harb Symp Quant Biol* **63**, 423-433 (1998).
- 687 9. A. L. Gartel, K. Shchors, Mechanisms of c-myc-mediated transcriptional repression of growth

- 688 arrest genes. *Exp Cell Res* **283**, 17-21 (2003).
- 689 10. B. Herkert, M. Eilers, Transcriptional repression: the dark side of myc. *Genes Cancer* **1**, 580-586  
690 (2010).
- 691 11. K. J. Campbell, R. J. White, MYC regulation of cell growth through control of transcription by  
692 RNA polymerases I and III. *Cold Spring Harb Perspect Med* **4**, (2014).
- 693 12. Z. A. Felton-Edkins *et al.*, Direct regulation of RNA polymerase III transcription by RB, p53 and c-  
694 Myc. *Cell Cycle* **2**, 181-184 (2003).
- 695 13. E. V. Prochownik, Regulation of Normal and Neoplastic Proliferation and Metabolism by the  
696 Extended Myc Network. *Cells* **11**, (2022).
- 697 14. E. V. Prochownik, H. Wang, Normal and Neoplastic Growth Suppression by the Extended Myc  
698 Network. *Cells* **11**, (2022).
- 699 15. L. R. Edmunds *et al.*, Abnormal lipid processing but normal long-term repopulation potential of  
700 myc<sup>-/-</sup> hepatocytes. *Oncotarget* **7**, 30379-30395 (2016).
- 701 16. L. R. Edmunds *et al.*, c-Myc and AMPK Control Cellular Energy Levels by Cooperatively  
702 Regulating Mitochondrial Structure and Function. *PLoS One* **10**, e0134049 (2015).
- 703 17. E. S. Goetzman, E. V. Prochownik, The Role for Myc in Coordinating Glycolysis, Oxidative  
704 Phosphorylation, Glutaminolysis, and Fatty Acid Metabolism in Normal and Neoplastic Tissues.  
705 *Front Endocrinol (Lausanne)* **9**, 129 (2018).
- 706 18. J. A. Graves *et al.*, Mitochondrial structure, function and dynamics are temporally controlled by c-  
707 Myc. *PLoS One* **7**, e37699 (2012).
- 708 19. Y. Gonskikh, N. Polacek, Alterations of the translation apparatus during aging and stress response.  
709 *Mech Ageing Dev* **168**, 30-36 (2017).
- 710 20. R. H. Houtkooper *et al.*, The metabolic footprint of aging in mice. *Sci Rep* **1**, 134 (2011).
- 711 21. F. Li *et al.*, Myc stimulates nuclearly encoded mitochondrial genes and mitochondrial biogenesis.  
712 *Mol Cell Biol* **25**, 6225-6234 (2005).
- 713 22. H. Wang *et al.*, Coordinated Activities of Multiple Myc-dependent and Myc-independent  
714 Biosynthetic Pathways in Hepatoblastoma. *J Biol Chem* **291**, 26241-26251 (2016).
- 715 23. H. Wang *et al.*, Premature aging and reduced cancer incidence associated with near-complete body-  
716 wide Myc inactivation. *Cell Rep* **42**, 112830 (2023).
- 717 24. H. Wang *et al.*, Disruption of Multiple Overlapping Functions Following Stepwise Inactivation of  
718 the Extended Myc Network. *Cells* **11**, (2022).
- 719 25. A. N. Billin, D. E. Ayer, The Mlx network: evidence for a parallel Max-like transcriptional network  
720 that regulates energy metabolism. *Curr Top Microbiol Immunol* **302**, 255-278 (2006).
- 721 26. P. Richards *et al.*, MondoA/ChREBP: The usual suspects of transcriptional glucose sensing;  
722 Implication in pathophysiology. *Metabolism* **70**, 133-151 (2017).
- 723 27. P. A. Carroll *et al.*, Deregulated Myc requires MondoA/Mlx for metabolic reprogramming and  
724 tumorigenesis. *Cancer Cell* **27**, 271-285 (2015).
- 725 28. H. Wang *et al.*, Myc and ChREBP transcription factors cooperatively regulate normal and  
726 neoplastic hepatocyte proliferation in mice. *J Biol Chem* **293**, 14740-14757 (2018).
- 727 29. H. Wang *et al.*, Coordinated Cross-Talk Between the Myc and Mlx Networks in Liver  
728 Regeneration and Neoplasia. *Cell Mol Gastroenterol Hepatol* **13**, 1785-1804 (2022).
- 729 30. Y. S. Jeong *et al.*, Integrated expression profiling and genome-wide analysis of ChREBP targets  
730 reveals the dual role for ChREBP in glucose-regulated gene expression. *PLoS One* **6**, e22544  
731 (2011).
- 732 31. D. Diolaiti, L. McFerrin, P. A. Carroll, R. N. Eisenman, Functional interactions among members of  
733 the MAX and MLX transcriptional network during oncogenesis. *Biochim Biophys Acta* **1849**, 484-  
734 500 (2015).
- 735 32. K. Iizuka, R. K. Bruick, G. Liang, J. D. Horton, K. Uyeda, Deficiency of carbohydrate response

- 736 element-binding protein (ChREBP) reduces lipogenesis as well as glycolysis. *Proc Natl Acad Sci U*  
737 *S A* **101**, 7281-7286 (2004).
- 738 33. S. Ishii, K. Iizuka, B. C. Miller, K. Uyeda, Carbohydrate response element binding protein directly  
739 promotes lipogenic enzyme gene transcription. *Proc Natl Acad Sci U S A* **101**, 15597-15602 (2004).
- 740 34. L. Ma, N. G. Tsatsos, H. C. Towle, Direct role of ChREBP.Mlx in regulating hepatic glucose-  
741 responsive genes. *J Biol Chem* **280**, 12019-12027 (2005).
- 742 35. X. Tong, F. Zhao, A. Mancuso, J. J. Gruber, C. B. Thompson, The glucose-responsive transcription  
743 factor ChREBP contributes to glucose-dependent anabolic synthesis and cell proliferation. *Proc*  
744 *Natl Acad Sci U S A* **106**, 21660-21665 (2009).
- 745 36. A. C. Davis, M. Wims, G. D. Spotts, S. R. Hann, A. Bradley, A null c-myc mutation causes  
746 lethality before 10.5 days of gestation in homozygotes and reduced fertility in heterozygous female  
747 mice. *Genes Dev* **7**, 671-682 (1993).
- 748 37. M. D. Bettess *et al.*, c-Myc is required for the formation of intestinal crypts but dispensable for  
749 homeostasis of the adult intestinal epithelium. *Mol Cell Biol* **25**, 7868-7878 (2005).
- 750 38. J. W. Hofmann *et al.*, Reduced expression of MYC increases longevity and enhances healthspan.  
751 *Cell* **160**, 477-488 (2015).
- 752 39. C. Rosselot *et al.*, Myc Is Required for Adaptive beta-Cell Replication in Young Mice but Is Not  
753 Sufficient in One-Year-Old Mice Fed With a High-Fat Diet. *Diabetes* **68**, 1934-1949 (2019).
- 754 40. E. V. Prochownik, H. Wang, Lessons in aging from Myc knockout mouse models. *Front Cell Dev*  
755 *Biol* **11**, 1244321 (2023).
- 756 41. L. Berben, G. Floris, H. Wildiers, S. Hatse, Cancer and Aging: Two Tightly Interconnected  
757 Biological Processes. *Cancers (Basel)* **13**, (2021).
- 758 42. M. Bertolotti *et al.*, Nonalcoholic fatty liver disease and aging: epidemiology to management.  
759 *World J Gastroenterol* **20**, 14185-14204 (2014).
- 760 43. T. Honma, M. Yanaka, T. Tsuduki, I. Ikeda, Increased lipid accumulation in liver and white  
761 adipose tissue in aging in the SAMP10 mouse. *J Nutr Sci Vitaminol (Tokyo)* **57**, 123-129 (2011).
- 762 44. H. Wang *et al.*, Structurally diverse c-Myc inhibitors share a common mechanism of action  
763 involving ATP depletion. *Oncotarget* **6**, 15857-15870 (2015).
- 764 45. L. Soucek *et al.*, Modelling Myc inhibition as a cancer therapy. *Nature* **455**, 679-683 (2008).
- 765 46. D. M. Muoio, Metabolic inflexibility: when mitochondrial indecision leads to metabolic gridlock.  
766 *Cell* **159**, 1253-1262 (2014).
- 767 47. J. Y. Jang, A. Blum, J. Liu, T. Finkel, The role of mitochondria in aging. *J Clin Invest* **128**, 3662-  
768 3670 (2018).
- 769 48. K. R. Short *et al.*, Decline in skeletal muscle mitochondrial function with aging in humans. *Proc*  
770 *Natl Acad Sci U S A* **102**, 5618-5623 (2005).
- 771 49. S. Zhu *et al.*, Aging- and obesity-related peri-muscular adipose tissue accelerates muscle atrophy.  
772 *PLoS One* **14**, e0221366 (2019).
- 773 50. A. Bowman, M. A. Birch-Machin, Age-Dependent Decrease of Mitochondrial Complex II Activity  
774 in Human Skin Fibroblasts. *J Invest Dermatol* **136**, 912-919 (2016).
- 775 51. G. Lenaz *et al.*, Mitochondrial complex I defects in aging. *Mol Cell Biochem* **174**, 329-333 (1997).
- 776 52. A. El-Gharbawy, J. Vockley, Inborn Errors of Metabolism with Myopathy: Defects of Fatty Acid  
777 Oxidation and the Carnitine Shuttle System. *Pediatr Clin North Am* **65**, 317-335 (2018).
- 778 53. J. Vockley, Long-chain fatty acid oxidation disorders and current management strategies. *Am J*  
779 *Manag Care* **26**, S147-S154 (2020).
- 780 54. A. Chadt, H. Al-Hasani, Glucose transporters in adipose tissue, liver, and skeletal muscle in  
781 metabolic health and disease. *Pflugers Arch* **472**, 1273-1298 (2020).
- 782 55. S. Rius-Perez, I. Torres-Cuevas, I. Millan, A. L. Ortega, S. Perez, PGC-1alpha, Inflammation, and  
783 Oxidative Stress: An Integrative View in Metabolism. *Oxid Med Cell Longev* **2020**, 1452696

- 784 (2020).
- 785 56. B. Ahn, The Function of MondoA and ChREBP Nutrient-Sensing Factors in Metabolic Disease. *Int*  
786 *J Mol Sci* **24**, (2023).
- 787 57. E. P. Consortium, The ENCODE (ENCyclopedia Of DNA Elements) Project. *Science* **306**, 636-640  
788 (2004).
- 789 58. T. V. Rohm, D. T. Meier, J. M. Olefsky, M. Y. Donath, Inflammation in obesity, diabetes, and  
790 related disorders. *Immunity* **55**, 31-55 (2022).
- 791 59. H. Wu, C. M. Ballantyne, Metabolic Inflammation and Insulin Resistance in Obesity. *Circ Res* **126**,  
792 1549-1564 (2020).
- 793 60. H. Wang *et al.*, Inhibition of hepatocellular carcinoma by metabolic normalization. *PLoS One* **14**,  
794 e0218186 (2019).
- 795 61. C. Tabula Muris, A single-cell transcriptomic atlas characterizes ageing tissues in the mouse.  
796 *Nature* **583**, 590-595 (2020).
- 797 62. J. R. Smith *et al.*, Relationship between in vivo age and in vitro aging: assessment of 669 cell  
798 cultures derived from members of the Baltimore Longitudinal Study of Aging. *J Gerontol A Biol*  
799 *Sci Med Sci* **57**, B239-246 (2002).
- 800 63. P. Zhang *et al.*, c-Myc is required for the CHREBP-dependent activation of glucose-responsive  
801 genes. *Mol Endocrinol* **24**, 1274-1286 (2010).
- 802 64. J. M. Snyder, J. M. Ward, P. M. Treuting, Cause-of-Death Analysis in Rodent Aging Studies. *Vet*  
803 *Pathol* **53**, 233-243 (2016).
- 804 65. P. J. Hurlin *et al.*, Deletion of Mnt leads to disrupted cell cycle control and tumorigenesis. *EMBO J*  
805 **22**, 4584-4596 (2003).
- 806 66. J. Liano-Pons, M. Arsenian-Henriksson, J. Leon, The Multiple Faces of MNT and Its Role as a  
807 MYC Modulator. *Cancers (Basel)* **13**, (2021).
- 808 67. G. Yang, P. J. Hurlin, MNT and Emerging Concepts of MNT-MYC Antagonism. *Genes (Basel)* **8**,  
809 (2017).
- 810 68. R. M. Russell, Factors in aging that effect the bioavailability of nutrients. *J Nutr* **131**, 1359S-1361S  
811 (2001).
- 812 69. P. Prasun, I. Ginevic, K. Oishi, Mitochondrial dysfunction in nonalcoholic fatty liver disease and  
813 alcohol related liver disease. *Transl Gastroenterol Hepatol* **6**, 4 (2021).
- 814 70. T. E. S. Kauppila, J. H. K. Kauppila, N. G. Larsson, Mammalian Mitochondria and Aging: An  
815 Update. *Cell Metab* **25**, 57-71 (2017).
- 816 71. S. Miwa, S. Kashyap, E. Chini, T. von Zglinicki, Mitochondrial dysfunction in cell senescence and  
817 aging. *J Clin Invest* **132**, (2022).
- 818 72. J. P. de Magalhaes, J. Curado, G. M. Church, Meta-analysis of age-related gene expression profiles  
819 identifies common signatures of aging. *Bioinformatics* **25**, 875-881 (2009).
- 820 73. D. H. Ly, D. J. Lockhart, R. A. Lerner, P. G. Schultz, Mitotic misregulation and human aging.  
821 *Science* **287**, 2486-2492 (2000).
- 822 74. S. Kim, Q. Li, C. V. Dang, L. A. Lee, Induction of ribosomal genes and hepatocyte hypertrophy by  
823 adenovirus-mediated expression of c-Myc in vivo. *Proc Natl Acad Sci U S A* **97**, 11198-11202  
824 (2000).
- 825 75. A. C. Ruifrok, D. A. Johnston, Quantification of histochemical staining by color deconvolution.  
826 *Anal Quant Cytol Histol* **23**, 291-299 (2001).
- 827 76. D. Kraus, Q. Yang, B. B. Kahn, Lipid Extraction from Mouse Feces. *Bio Protoc* **5**, (2015).
- 828 77. A. I. Mina *et al.*, CalR: A Web-Based Analysis Tool for Indirect Calorimetry Experiments. *Cell*  
829 *Metab* **28**, 656-666 e651 (2018).
- 830 78. M. J. Zhang, A. O. Pisco, S. Darmanis, J. Zou, Mouse aging cell atlas analysis reveals global and  
831 cell type-specific aging signatures. *Elife* **10**, (2021).

- 832 79. A. Subramanian *et al.*, Gene set enrichment analysis: a knowledge-based approach for interpreting  
833 genome-wide expression profiles. *Proc Natl Acad Sci U S A* **102**, 15545-15550 (2005).  
834 80. E. Y. Chen *et al.*, Enrichr: interactive and collaborative HTML5 gene list enrichment analysis tool.  
835 *BMC Bioinformatics* **14**, 128 (2013).  
836 81. T. Wu *et al.*, clusterProfiler 4.0: A universal enrichment tool for interpreting omics data. *Innovation*  
837 *(Camb)* **2**, 100141 (2021).  
838

### 839 Acknowledgements

840 **Funding:** The analysis of RNAseq and other genomics data was, in part, supported by the University of  
841 Pittsburgh Center for Research Computing. Specifically, this work utilized the HTC cluster, which is  
842 funded by NIH award number S10OD028483. Additionally, funding for this project was provided by NIH  
843 grant RO1 CA174713, The Rally Foundation (grant no. 22N42), and a Hyundai Hope on Wheels Scholar  
844 grant, all awarded to EVP.  
845

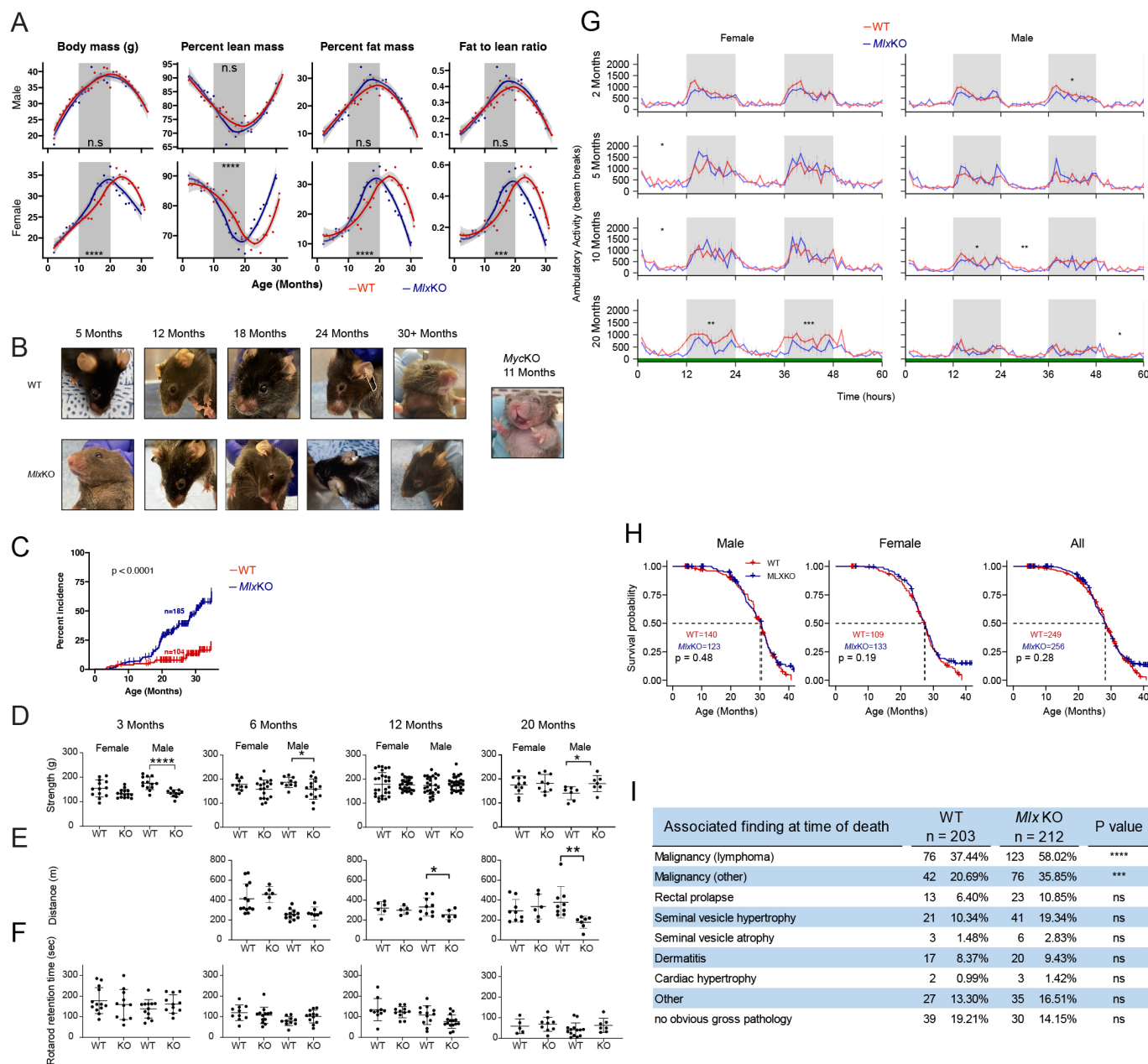
846 **Author contributions:** The analysis of RNAseq and other genomics data was, in part, supported by the  
847 University of Pittsburgh Center for Research Computing. Specifically, this work utilized the HTC cluster,  
848 which is funded by NIH award number S10OD028483. Additionally, funding for this project was provided  
849 by NIH grant RO1 CA174713, The Rally Foundation (grant no. 22N42), and a Hyundai Hope on Wheels  
850 Scholar grant, all awarded to EVP.  
851

852 **Declaration of interests:** The authors declare no competing interests.  
853

854 **Data and materials availability:** All data needed to evaluate the conclusions in the paper are present in  
855 the paper and/or the Supplementary Materials. All raw RNA-seq files have been deposited in the NCBI  
856 Gene Expression Omnibus and are accessible through GEO Series accession number GSE248073 and  
857 GSE223676.  
858  
859

860 **Figures and Tables**

861



862

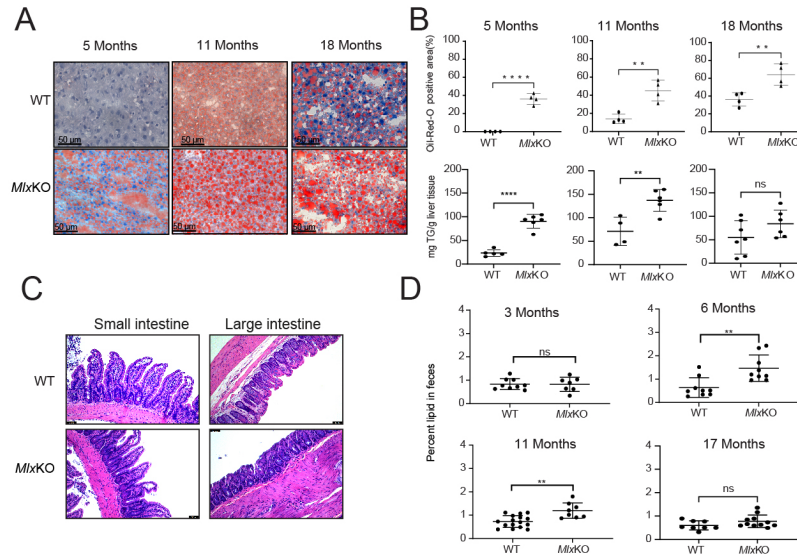
863

864 **Figure 1. *Mlx*KO mice show attributes of premature aging and a higher cancer incidence but have**  
865 **normal lifespans.**

866 **(A)** Weight and body composition of WT and *Mlx*KO mice during the course of life. Measurements were made  
867 as previously described beginning at the time of weaning when the *Mlx* gene was first inactivated (23). Total  
868 body fat and lean mass content were determined by EchoMRI scanning at the time of weighing. Each point  
869 represents the mean of measurements from 10-20 animals performed over the course of 2-3 days. Significant  
870 differences between the 2 groups are indicated by areas of shading. \*= $P < 0.05$ , \*\*= $P < 0.01$ ; \*\*\*= $P < 0.001$ ;  
871 \*\*\*\*= $P < 0.0001$ .

872 **(B)** Overall appearance of *Mlx*KO mice at various ages along with age-matched WT mice. Note typical  
873 examples of corneal opacifications (leucoma simplex). The image at the extreme right shows an example of an  
874 11 month old *Myc*KO mouse displaying substantial graying and loss of fur (23).

- 875 **(C)** Cumulative occurrence of both unilateral and bilateral leucoma simplex in WT and *Mlx*KO mice.
- 876 **(D)** Grip strength of WT and *Mlx*KO mice at the indicated ages.
- 877 **(E)** Treadmill endurance testing of WT and *Mlx*KO mice at the indicated ages.
- 878 **(F)** Rotarod testing of WT and *Mlx*KO mice at the indicated ages. In **D-F**, each point represents the mean of 3
- 879 tests performed on the same mouse on consecutive days.
- 880 **(G)** Total diurnal ambulatory activity in 5 month old 18 month old WT and *Mlx*KO mice measured in
- 881 metabolic cages (23).
- 882 **(H)** Survival of WT and *Myc*KO mice.
- 883 **(I)** Pathologies associated with WT and *Mlx*KO mice at the time of death.
- 884



885

886 **Figure 2. *MlxKO* prematurely accumulate excessive hepatic lipids and show evidence of dietary fat**  
887 **malabsorption.**

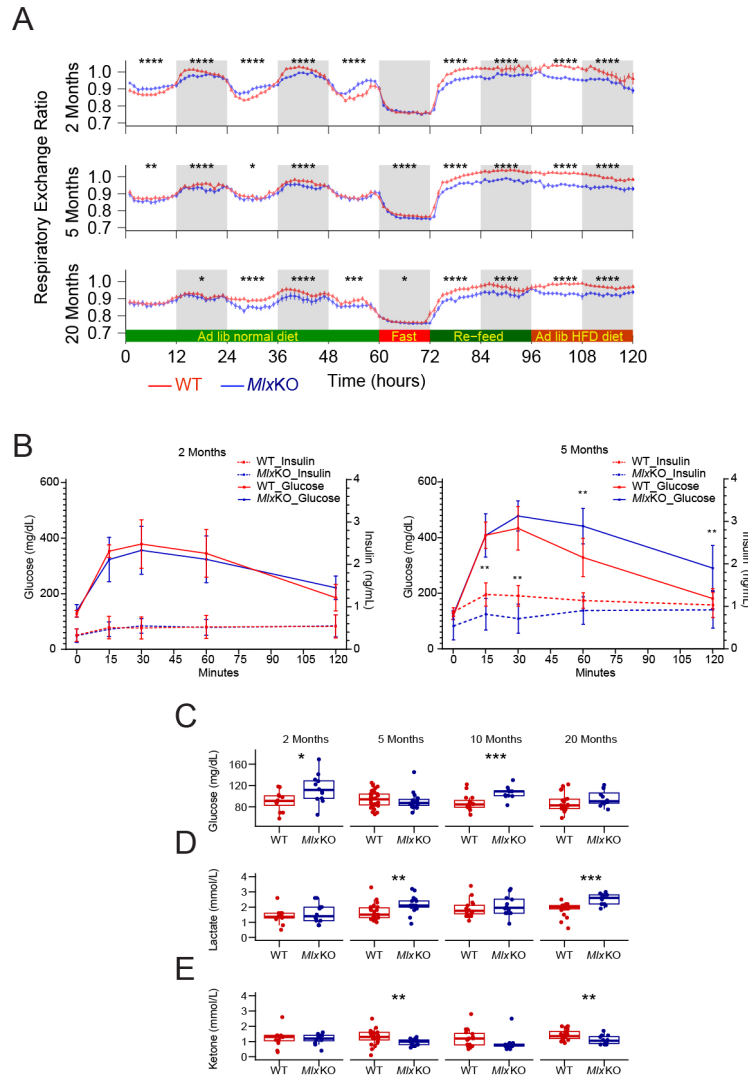
888 (A) ORO staining of livers from WT and *MlxKO* mice of the indicated ages

889 (B) Triglyceride content in the livers of mice similar to those depicted in A

890 (C) H&E-stained sections of small and large intestines of WT and *MlxKO* mice of the indicated ages

891 (D) Fecal fat content from WT and *MlxKO* mice of the indicated ages. Fecal fat was collected over 48-72 hr  
892 from individually caged mice maintained on standard diets.

893



894

895 **Figure 3. Metabolic alterations in *MlxKO* mice.**

896 **(A)** Respiratory exchange ratios in WT and *MlxKO* mice performed in metabolic cages at the indicated ages.

897 N=11-12 animals/group.

898 **(B)** GTTs performed on WT and *MlxKO* mice at the indicated ages. Glucose was administered via i.p  
899 injection to fasting animals animals as previously described (23). N=5 animals/group.

900 **(C,D,E)** Fasting serum glucose, lactate and ketone levels, respectively performed on WT and *MlxKO* mice at  
901 the indicated ages.

902



905 **Figure 4. Aberrant Mitochondrial Function in *Mlx*KO tissues.**

906 **(A,B,C)** Respirometry studies on mitochondria from liver, adipose tissue and skeletal muscle, respectively of  
907 5 month WT and *Mlx*KO mice in response to malate, pyruvate, palmitoyl-CoA and total Complex I and  
908 Complex II activities.

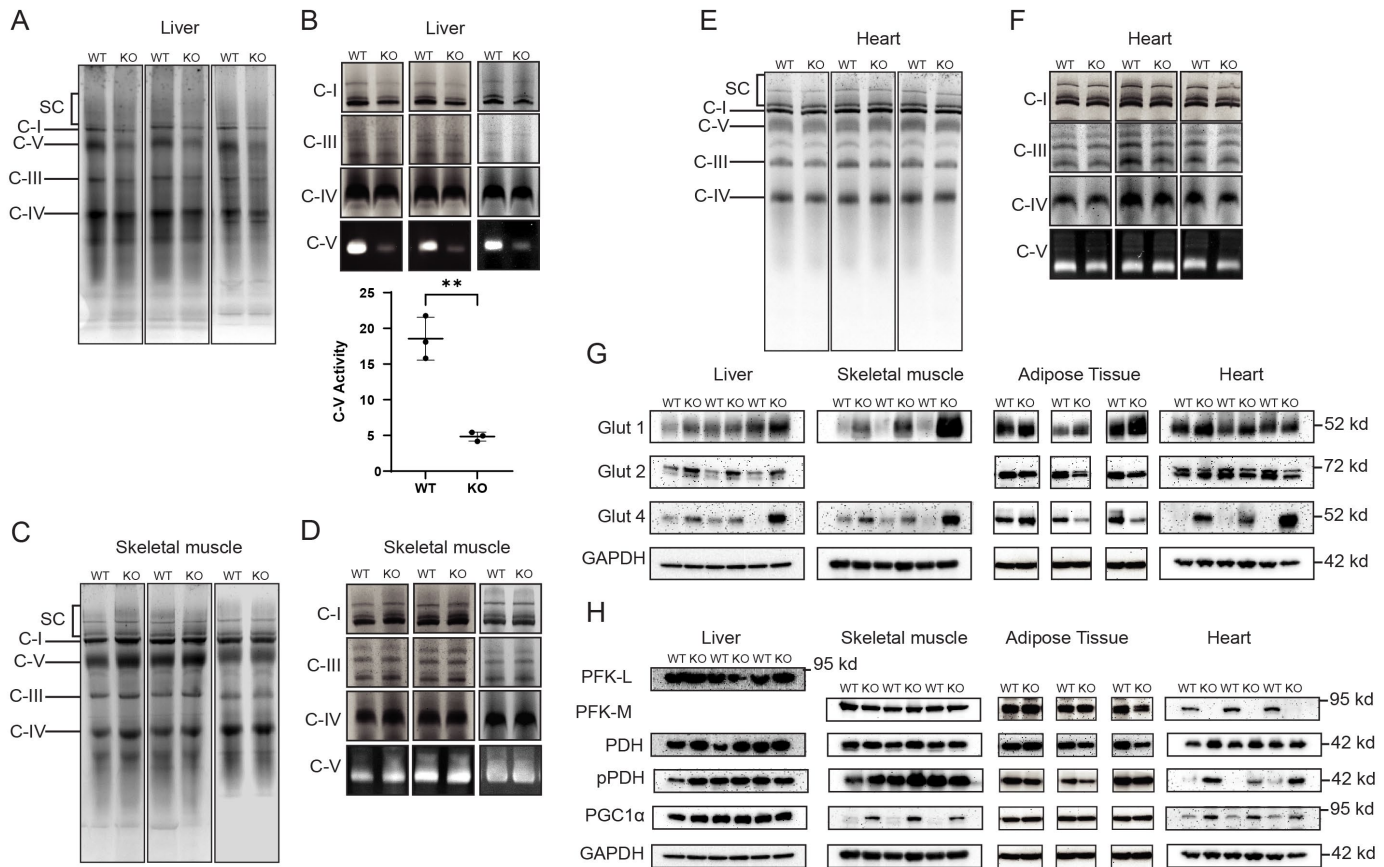
909 **(D,E,F)** Respirometry studies as described in A-C performed on 20 month old mice

910 **(G,H)** Serum acyl carnitine levels in 5 month old and 20 month old WT vs. *Mlx*KO mice, respectively.

911 Significant differences between the two groups are highlighted in red along the horizontal axis.

912 **(I,J)** Comparison of serum acyl carnitine levels in 5 month old vs. 20 month old WT and *Mlx*KO mice,  
913 respectively. Significant differences between the two groups are highlighted in red along the horizontal axis.

914



915

916 **Figure 5. *MlxKO* tissues are associated with selective changes in mitochondrial function.**

917 **(A)** BNGE of purified ETC Complexes I-V and ATP synthase (Complex V) from WT and *MlxKO* livers of 5  
918 month old mice. SC: supercomplexes.

919 **(B)** *In situ* enzymatic activities of the Complexes shown in **A** (18). In the graph below the image, relative  
920 specific activities of Complex V were quantified by normalizing scans of enzymatic reactions to the  
921 Coomassie Blue-stained bands in **A**.

922 **(C)** BNGE of purified ETC Complexes I-V and ATP synthase (Complex V) from WT and *MlxKO* skeletal  
923 muscle of 5 month old mice.

924 **(D)** *In situ* enzymatic activities of the Complexes shown in **C**.

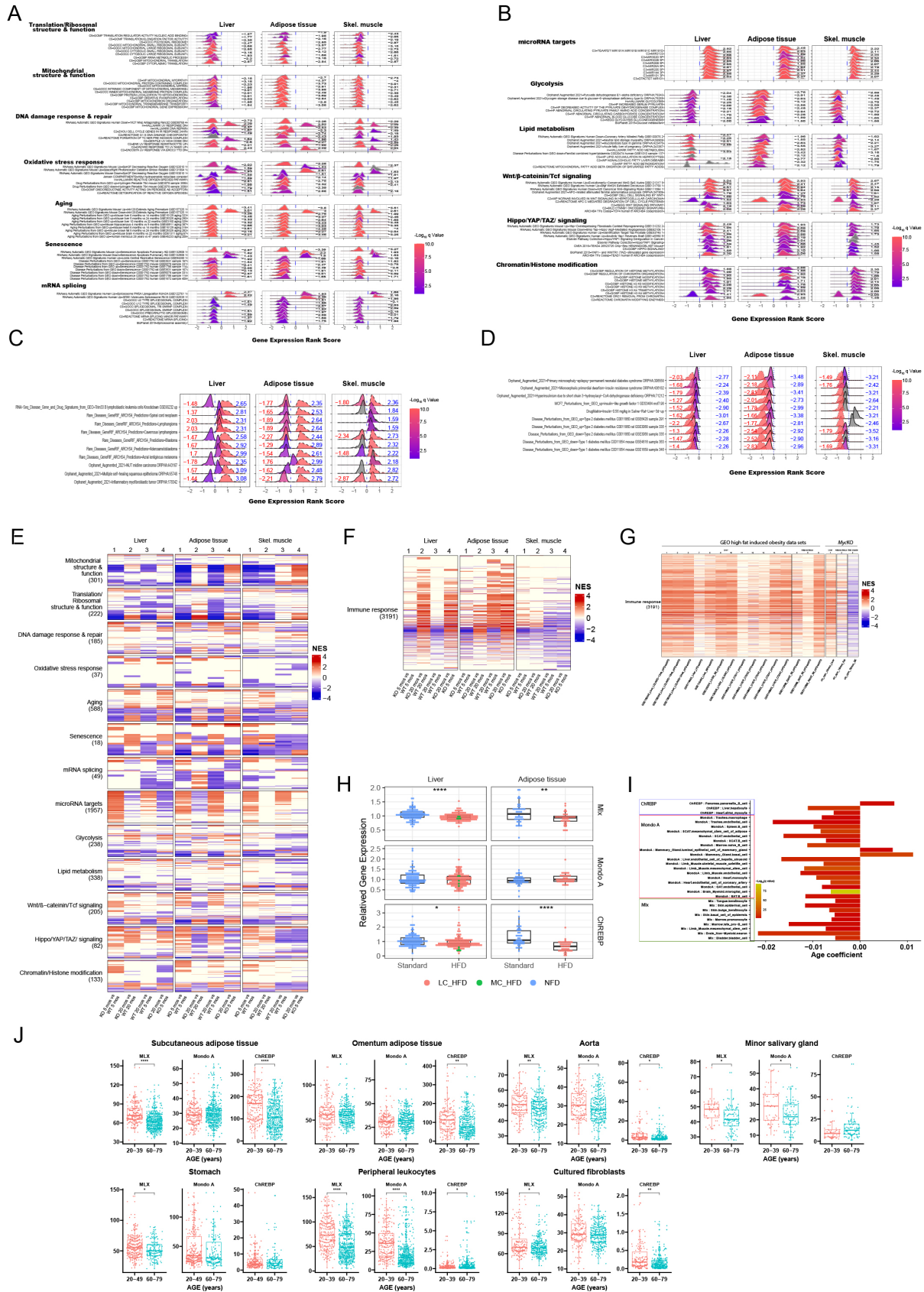
925 **(E)** BNGE of purified ETC Complexes I-V and ATP synthase (Complex V) from WT and *MlxKO* hearts of 5  
926 month old mice.

927 **(F)** *In situ* enzymatic activities of the Complexes shown in **E**.

928 **(G)** Immunoblots of select glucose transporters in the indicated tissues from 5 month old WT and *MlxKO*  
929 mice. The absence of a Glut2 panel for skeletal muscle indicates that the protein was not detected in that  
930 tissue

931 **(H)** Immunoblots of the indicated factors in WT and *MlxKO* tissues.

932



935 **Figure 6. Transcriptional analysis of *Mlx*KO tissues identifies unique targets as well as those previously**  
936 **identified as being *Myc*-regulated.**

937 **(A)** The EnrichR and MSigDB databases were searched to identify gene sets in *Mlx*KO liver, abdominal  
938 adipose tissue and skeletal muscle that were selectively enriched relative to WT mice (N=5 tissues/group).  
939 ClusterProfiler and the ridgeline plot application tool (80, 81). were used to display representative examples  
940 of these differentially enriched gene sets from 7 functional categories whose component gene sets were  
941 enriched in the same tissues from 5 month old *Myc*KO mice. Numbers to the right of each profile indicate the  
942 normalized enrichment score (NES) for that gene set. Gray curves and the absence of an NES indicate gene  
943 sets that were not significantly enriched in that tissue but were enriched in at least one other. NESs >0  
944 represent gene sets that were up-regulated relative to their corresponding WT tissue whereas NESs <0  
945 indicate gene sets that were up-regulated. See Supplementary Figures 3-9 for actual GSEA profiles for these  
946 and other gene sets and Supplementary File 1 for a complete list of all significantly enriched gene sets  
947 identified from the above-mentioned tissues of *Mlx*KO mice.

948 **(B)** Ridgeline plots of individual gene sets, comprising 6 functional categories, selectively enriched in the  
949 indicated *Mlx*KO tissues (See Supplementary Figures 10-15 for actual GSEA profiles for these and other gene  
950 sets contained within these categories and Supplementary File 2 for a complete list of all significantly  
951 enriched gene sets.

952 **(C)** Ridgeline plots of individual gene sets related to cancer in each of the indicated *Mlx*KO and *Myc*KO  
953 tissues. Dotted curves, whose NESs are indicated in blue, represent the gene set profiles from *Mlx*KO tissues  
954 and solid curves, whose NESs are indicated in red, represent gene set profiles from *Myc*KO tissues. See  
955 Supplementary Figures 16 and 17 for actual GSEA profiles and Supplementary file 3 for a list of all cancer-  
956 related gene sets identified as being enriched in the above tissues.

957 **(D)** Ridgeline plots for individual gene sets dysregulated in T1D and T2D represented as shown in C.

958 **(E)** Heat map of gene sets from the categories shown in panels A and B along with a more extensive  
959 collection of gene sets with significant enrichment scores. The total number of gene sets in each category in  
960 indicated beneath its name and their identities are indicated in Supplementary File 4.

961 **(F)** Heat map of 3191 gene sets pertaining to the immune response, inflammation and cytokine production  
962 that were significantly dysregulated in *Mlx*KO tissues from 20 month old mice versus matched WT tissues.

963 **(G)** Enrichment of differentially expressed gene sets from F in liver, adipose tissue and skeletal muscle from  
964 adult mice maintained on standard or various types of HFDs for 10-24 weeks. The right-most 3 columns  
965 show GSEA differences between WT and *Myc*KO tissues (n=5 tissues/group) (23).

966 **(H)** *Mlx*, *MondoA* and *ChREBP* transcript levels in the livers and adipose tissues from mice maintained on  
967 the standard diets or HFDs described in G.

968 **(I)** scRNA-seq results for *MondoA*, *ChREBP* and *Mlx* expression from the Tabula Muris Consortium  
969 database (61) consisting of 90 sc populations from 23 different tissues of young (1-3 months) and old (18-30  
970 months) mice. Results are expressed as q values that were calculated from correlation coefficients that  
971 compared transcript levels across aging populations.

972 **(J)** Age-related declines in *MondoA*, *ChREBP* and *Mlx* transcripts in select human tissues and cultured  
973 primary fibroblasts. RNA seq results were divided into those obtained from younger (20-49 years) and older  
974 (60-79 years) individuals.